



UNIVERSITY OF LEEDS

This is a repository copy of *Synthesis of Ti(SO₄)O solid acid nano-catalyst and its application for biodiesel production from used cooking oil*.

White Rose Research Online URL for this paper:
<http://eprints.whiterose.ac.uk/104400/>

Version: Accepted Version

Article:

Gardy, J, Hassanpour, A orcid.org/0000-0002-7756-1506, Lai, X et al. (1 more author) (2016) Synthesis of Ti(SO₄)O solid acid nano-catalyst and its application for biodiesel production from used cooking oil. *Applied Catalysis A: General*, 527. pp. 81-95. ISSN 0926-860X

<https://doi.org/10.1016/j.apcata.2016.08.031>

© 2016, Elsevier. Licensed under the Creative Commons Attribution-NonCommercial-NoDerivatives 4.0 International
<http://creativecommons.org/licenses/by-nc-nd/4.0/>

Reuse

Unless indicated otherwise, fulltext items are protected by copyright with all rights reserved. The copyright exception in section 29 of the Copyright, Designs and Patents Act 1988 allows the making of a single copy solely for the purpose of non-commercial research or private study within the limits of fair dealing. The publisher or other rights-holder may allow further reproduction and re-use of this version - refer to the White Rose Research Online record for this item. Where records identify the publisher as the copyright holder, users can verify any specific terms of use on the publisher's website.

Takedown

If you consider content in White Rose Research Online to be in breach of UK law, please notify us by emailing eprints@whiterose.ac.uk including the URL of the record and the reason for the withdrawal request.



eprints@whiterose.ac.uk
<https://eprints.whiterose.ac.uk/>

Synthesis of $\text{Ti}(\text{SO}_4)\text{O}$ solid acid nano-catalyst and its application for biodiesel production from used cooking oil

Jabbar Gardy¹, Ali Hassanpour^{1,*}, Xiaojun Lai¹, Mukhtar H. Ahmed²

¹School of Chemical and Process Engineering, University of Leeds, LS2 9JT Leeds, UK.

²Nanotechnology Integrated Bioengineering Centre, University of Ulster, Jordanstown, BT37 0QB Belfast, UK.

*Tel.: +441133432405; E-mail: a.hassanpour@leedsus.ac.uk

ABSTRACT

A novel solid acid nano-catalyst [$\text{Ti}(\text{SO}_4)\text{O}$] was synthesised and used for the simultaneous esterification and transesterification of free fatty acids in used cooking oil (UCO) to produce biodiesel. The synthesised nano-catalyst was fully characterised by different analytical techniques. The XPS results clearly confirmed that the bidentate sulphate coordinated to the Ti^{4+} metal in the nano-catalyst product. Obtained d-spacing values from the experimental data of XRD peaks and the SAED pattern of produced nano-catalyst agreed well with the d-spacing values from the JCPDS-ICDD card numbers 04-011-4951 for titanium sulphate oxide or titanium oxysulfate crystal structures. This confirms the sulphate groups were within the crystalline structure rather than on the surface of titania nano particles, which has not been previously reported. It has been demonstrated 97.1% yield for the fatty acid methyl ester can be achieved using the synthesised catalyst under a reaction time of 3 hrs, catalyst to UCO ratio of 1.5wt% and methanol to UCO ratio of 9:1 at 75°C reaction temperature. The nano-catalyst showed a good catalytic activity for the feedstock containing ≤ 6 wt% free fatty acid. Furthermore, the catalytic activity and re-usability of the $\text{Ti}(\text{SO}_4)\text{O}$ for the esterification/transesterification of UCO were investigated. XRD results confirmed that the amount of SO_4^{2-} species in the solid acid nano-catalyst slowly decreased with re-use after 8 cycles under optimized conditions, which is higher than the reusability of other functionalised titania reported in the literature. Finally, the biodiesel produced from this process satisfied the ASTM and European Norm standards.

Key words

Titanium sulphate oxide or titanium oxysulfate; solid acid catalyst; esterification & transesterification process; used cooking oil; nano-catalyst; and biodiesel.

1. INTRODUCTION

During past twenty years, scientists have been investigating alternatives to fossil fuels in to meet global energy demands and reduce carbon emissions. Biodiesel has been widely regarded as a suitable resource because of its availability [1], renewability [2], lower gas emissions [3], non-toxicity [4], and its biodegradability [2, 5]. Currently around 90% of biodiesel is produced by the transesterification process of triglycerides with low molecular weight alcohols using homogenous acid or base catalysts. However, the biodiesel industry faces some significant challenges; (i) high cost of biodiesel feedstock (70 to 85% of the overall production cost) and (ii) cost of biodiesel processing, including separation, purification and neutralisation of by-products [6-9]. These issues can be resolved by using low-cost feedstocks, but with catalysts highly tolerant to moisture and Free Fatty Acids (FFA) in oil, because FFA and moisture content in cheap raw materials have an adverse effect on catalyst activity.

Used Cooking Oil (UCO) is regarded as the a promising feedstock for biodiesel production despite containing a certain amount of water, a large amount of FFA and other impurities [10, 11]. If UCO contains more than 1.0% of FFA and 0.5% of water, a homogenous based catalyst would not be preferred in the transesterification process because of soap formation (fatty acid salts), hydrolysis of the product and decreasing the reactivity of the base catalyst [12, 13]. One way of reducing the amount of FFA is to use a homogenous acidic catalyst for the pre-esterification of UCO; however, using an acidic catalyst demands expensive equipment to avoid acid corrosion, which inevitably increases costs of biodiesel production [2, 14]. Heterogeneous catalysts, however, could be suitable for biodiesel production from UCO due to their reusability, higher stability, high surface area, non-toxicity and the simplicity of purification as reported by other researchers [15-20]. Numerous

studies have been conducted on the development of sulphated metal oxides for the simultaneous esterification and transesterification process of UCO to produce biodiesel [21-23]. Several synthetic routes were applied for the preparation of heterogeneous catalysts including sol-gel [24-27], solvent-free [28, 29] and hydrothermal methods [30-33]. Examples of heterogeneous catalysts include $\text{SO}_4^{2-}/\text{TiO}_2$ [30, 34-37], $\text{SO}_4^{2-}/\text{TiO}_2\text{-SiO}_2$ [38-41], $\text{SrO}/\text{SO}_4^{2-}\text{-ZrO}_2$ [29], $\text{SO}_4^{2-}/\text{ZrO}_2$ [17, 42-44], $\text{SO}_4^{2-}/\text{TiO}_2\text{-ZrO}_2$ [45] and $\text{SO}_4^{2-}/\text{SnO}_2$ [17, 46], which were considered for a good catalytic activity for the raw materials containing large amounts of FFA in biodiesel production. Among these, sulphated doped TiO_2 is a good example of a solid super-acidic catalyst which is also used in the petrochemical industry and petroleum refining process [24, 47] and showed better performances as compared to other sulphated metal oxides. This is due to the acid strength of the TiO_2 particles which further enhances with loading of SO_4^{2-} groups on the surface of TiO_2 [48]. Many recent studies have reported that the super acidity of sulphated titanium dioxide catalysts could be based on Lewis acid and Brønsted acid sites, and the formation of Brønsted acid sites are possibly due to the higher content of sulphate groups in the catalyst [24, 49, 50]. The presence of Brønsted acid sites in acid catalysts is significantly important for the catalytic activity [28, 51, 52]. Some researchers have reported that the addition of sulphate ions to metal oxides enhances the acidic properties, catalytic activity, high selectivity, and causes less deactivation of the catalyst [25, 53-56]. However, Shi and Li [36] observed the deposition of carbon on the surface of sulphated metal oxide catalysts is the main reason to poison the catalytic activity of sulphated titania.

Chen, et al. [34] studied transesterification of cotton seed oil at 230°C with 12:1 methanol to oil ratio for 8 hrs reaction time using 2wt% of $\text{SO}_4^{2-}/\text{TiO}_2$ catalyst to achieve 90% biodiesel. Furthermore, Roper-Vega et al. [35] investigated the effect of $\text{SO}_4^{2-}/\text{TiO}_2$ on the esterification of oleic acid with ethanol. They found that the maximum conversion of oleic acid was 82.2%, whilst a 100% selectivity of the catalyst on oleic acid to ester was reported at 80°C after 3hrs. Zhao and co-workers [30] have recently studied the catalytic activity of sulphated titanium oxide ($\text{SO}_4^{2-}/\text{TiO}_2$) with exposed (001)

and (101) facets for esterification of acetic acid and n-butanol. It was reported that the high surface acidity of titanium dioxide ($\text{SO}_4^{2-}/\text{TiO}_2$) increased the yield of butyl acetate to about 92.2% in esterification reaction and the selectivity of the catalyst mostly depended on the degree of exposure of reactive crystal facets. Yang et al. [40] reported a novel strategy for the preparation of $\text{SO}_4^{2-}/\text{TiO}_2\text{-SiO}_2$ nano-crystalline solid catalyst. The prepared nano-catalyst had a high surface area of $550\text{m}^2/\text{g}$ compared to $\text{SO}_4^{2-}/\text{TiO}_2$ nano-catalyst. Nonetheless, the catalyst displayed low catalytic activity for glycerine with acetic acid in toluene at 120°C . Peng et al. [38] reported a study on the use of $\text{SO}_4^{2-}/\text{TiO}_2\text{-SiO}_2$ as a solid acid catalyst for the simultaneous esterification and transesterification of low cost feedstocks with high FFA. They reported that under 9:1 methanol to oil molar ratio, 6hrs reaction time, 3% catalyst loading, and reaction temperature of 200°C a yield of 92% can be achieved. It was also reported that the $\text{SO}_4^{2-}/\text{TiO}_2\text{-SiO}_2$ catalyst can be re-used up to 4 times without reducing the catalytic activity. Recently, an inexpensive precursor was used in the synthesis of $\text{SO}_4^{2-}/\text{TiO}_2\text{-SiO}_2$ catalyst by Shao and co-workers [41]. They reported 88% yield for biodiesel production under 20:1 methanol to UCO molar ratio, 10wt% catalyst concentration and 3hrs reaction time at 120°C with constant stirring at 400rpm. Nurul Hajar et al. [39] have recently used $\text{SO}_4^{2-}/\text{TiO}_2\text{-SiO}_2$ catalyst for the transesterification of decanter cake produced from waste palm oil into biodiesel. It was found that 120°C reaction temperature, 1:15 oil to methanol ratio, 5hrs transesterification time, and 13wt% catalyst loading a 91% yield was achieved.

The stability and catalytic activity of sulfated metal oxide catalysts strongly depended on the synthetic routes, sulfate content and the position of sulfate group in the structure of the catalyst. Few researchers [57] have recently reported the addition of rare earth element, such as La^{+3} and Ce^{+3} , could enhance the catalytic stability of the sulphated TiO_2 for the simultaneous esterification and transesterification of waste cooking oil [48, 58]. The application of such catalysts is preferable in simultaneous esterification and transesterification reactions when using cheap raw materials with high FFA due to the high acidity of solid acid catalysts. The major drawback with the sulphated

metal oxide catalysts could be (i) relatively high temperature requirements, (ii) low yield, (iii) long reaction time and (iv) catalyst stability and reusability [59]. The latter could be due to the fact that the sulphate group is placed on the surface of the catalysts in majority of cases, making the catalyst prone to deactivation. The present work describes a novel method of preparing $\text{Ti}(\text{SO}_4)\text{O}$ solid super acidic nano-catalyst, where the sulphate group is chemically bonded within the structure of the catalyst with potential high stability and reusability. Characterisation and application of the developed nano-catalyst for biodiesel production via simultaneous esterification and transesterification of used cooking oil (UCO) are investigated; because, so far, there is no reported work and/or information available on the nano catalysts of titanium sulphate oxide or titanium oxide sulfate [$\text{Ti}(\text{SO}_4)\text{O}$] for biodiesel production. The chemical structure, catalytic stability, morphology, particle sizes and surface area for the catalyst are determined using X-ray diffraction (XRD), Fourier transform infrared (FT-IR) spectroscopy, X-ray photoelectron spectroscopy (XPS), N_2 adsorption-desorption isotherms, scanning electron microscopy (SEM), transmission electron microscopy (TEM), and thermogravimetric analysis coupled with FT-IR (TGA-FTIR). The effect of catalyst loading, time and temperature of reaction, methanol to UCO ratio and level of FFA in the feedstock on the biodiesel yield as well as the catalyst activity and stability during the esterification/transesterification are investigated. Additionally, the obtained biodiesel from the catalytic transesterification processes is analysed in accordance to ASTM and EN standard methods to determine characteristic fuel properties such as kinematic viscosity, cloud point, density, flash point, fatty acid methyl ester (FAME) content, linoleic acid methyl ester (LAME) content, and acid number.

2. EXPERIMENTAL

2.1 Materials

The sample of UCO provided by a restaurant in Leeds, UK, was used as a cheap raw material. The feedstock was pre-treated by filtration to remove impurities through filter paper and heated to 100°C

to minimise the moisture in the esterification/transesterification process. The physicochemical properties of pre-treated UCO, presented in Table S1 (supplementary information), were measured using EN and ASTM standard methods. Oleic acid and chlorosulfonic acid (for preparation of catalyst) were obtained from Fluka Analytical. Titanium (IV) oxide (99.5% purity), methanol (≥ 99.9 purity), methyl heptadecanoate (≥ 99.5 purity, internal standard for GC), FAME mix reference standard (99.9 purity, GC), n-heptane (≥ 99 purity, GC), acetone and n-hexane (99.5%, purity) were purchased from Sigma-Aldrich (UK) and used without further purifications.

2.2 Methodology

2.2.1 Synthesis of $\text{Ti}(\text{SO}_4)_2$ nano-catalyst

The titanium sulphate oxide or titanium oxysulphate nano-catalyst has been prepared using following procedure: 17.16mmol of chlorosulfonic acid was added drop-wise using a glass syringe at room temperature into a round-bottomed flask containing 5.0g of titanium (IV) oxide. The resulting mixture was then heated on an automatic hotplate-magnetic stirrer at 120°C using agitation rate of 500RPM, to prevent generation of hydrogen and chloride gases in the flask. The flask containing the produced gel solution was connected with a reflux condenser using tap water to condensate the remaining reagent for 2 hours at the constant stirring rate. The resulting gel solution aged quiescently at room temperature for 2 hours and was then dried in an oven at 110°C overnight. The resultant catalyst was crushed and grinded by pestle mortar, and then the grinded powders were washed properly with 1:1 ratio of acetone to n-hexane in order to remove any remaining residues on the surface of the prepared catalyst. Finally, the obtained fine powder was dried in an oven at 110°C in order to remove any moisture on the surface of the catalyst, then characterized, using different analytical tools to determine the chemical structure, morphology, surface area, thermal/oxidative stability and particle sizes.

2.2.2 Synthesis and analysis of biodiesel fuel

The simultaneous esterification and transesterification of UCO was performed in a glass batch reactor connected with an automatic temperature controller loop system (Ministat Huber 125 Pilot ONE Controller, UK) under constant agitation rate at 600RPM using a digital mechanical stirrer (Eurostar digital IKA) and a reflux condenser. Specified amounts of nano-catalyst, pre-treated UCO and methanol were charged into the batch reactor. The three-phase mixture was agitated and heated to specified temperatures and times. The final reaction mixture was poured into a separating funnel and allowed to cool down to ambient temperature. The crude methyl ester, contained in the upper layer, was separated by gravity from the glycerol layer and nano-catalyst in the lower layer. The crude biodiesel layer was then separated from any remaining nano-catalyst and glycerol by a centrifuge at 9000RPM for 10 minutes.

The FAME content of the prepared biodiesel sample was quantified by Perkin Elmer Clarus gas chromatography (580S, GC), equipped with a mass spectroscopy (560S, MS) instrument. The chromatographic separation was achieved on an Elite 5MS capillary column (30.0m x 250 μ m) and helium was used as a carrier gas at a constant flow rate of 1ml per minute. The initial oven temperature in the column was programmed at 60°C for 0min then ramped to 200°C at 10°C/min. The temperature was held for 10min at 200°C then increased to 270°C at 10°C/min. Finally, the temperature was held for 5 minutes to remove any remaining traces of sample residue. Biodiesel sample was injected in splitless mode with a split ratio of 2:1. The transfer line temperature and the injection temperature were kept at 250°C. GC-MS was operated in the 70eV electron ionization mode with a collected scanning mass range of 50 to 600Da. The GC instrument was calibrated using a reference FAME mixture and the biodiesel sample was prepared by dissolving (250 \pm 5) mg in 5mL of solution of internal standard with n-heptane using a shaker. 1.0mL of the prepared solution of the sample was transferred into 2.0ml of GC automatic sampler vial for injection, followed by the instrument injecting automatically 0.5 μ l of this solution into the GC instrument. Turbo MassTM

software was used for data processing and reporting. The method to calculate the percentage of total FAMES has been reported elsewhere [60] and the FAME composition result for obtained biodiesel is presented in Table 1.

Table 1 Fatty acid methyl ester composition for obtained UCO biodiesel

FAME	Form	wt% content
Palmitic acid methyl ester	C _{16:0}	6.23
Stearic acid methyl ester	C _{18:0}	0.85
Oleic acid methyl ester	C _{18:1}	69.56
Linoleic acid methyl ester	C _{18:2}	20.41
Linolenic acid methyl ester	C _{18:3}	2.18
Arachidic acid methyl ester	C _{20:0}	0.17
Gadoleic acid methyl ester	C _{20:1}	0.31
Erucic acid methyl ester	C _{21:1}	0.16
Behenic acid methyl ester	C _{22:0}	0.12

The separated nano-catalyst was properly washed three times with 1:1 ratio of methanol to n-hexane in order to remove any remaining non-polar and polar compounds on its surface such as fatty acid methyl ester (FAME), glycerol, monoglycerides, diglycerides and triglycerides. Finally, the catalyst was treated in an oven for 3hrs at 110°C to remove any moisture on the surface then the structure of the nano-catalyst was re-confirmed using XRD before it was re-used in order to determine the nano-catalyst life time.

2.2.3 Characterization methods

2.2.3.1 Catalyst characterization

The XRD patterns of the nano-catalyst samples were obtained using Bruker D8 X-ray diffraction fitted with a LynxEye detector, using CuK α (1.54Å) radiation source operating at 40kV and 40mA,

calibrated against a Si standard. Each sample was scanned from 2θ angle ranging 10° to 70° with step size 0.0495° at 35 seconds per step.

Fourier transform infrared (FT-IR) spectroscopy of original TiO_2 -NPs and synthesized $\text{Ti}(\text{SO}_4)_2$ nano-catalyst were carried out at room temperature using a Nicolet iS10 FT-IR spectrometer equipped with a deuterated triglycine sulfate (DTGS) KBr detector to investigate the chemical vibrational modes in each catalyst sample. A minimum of 36 scans were performed at the average signal of infrared with a resolution 4cm^{-1} in the ranges of 400 cm^{-1} to 4000cm^{-1} . The X-ray photoelectron spectroscopy (XPS) was carried out using a KRATOS XSAM 800 fitted with an energy analyser. The X-ray source employed was Al- $K\alpha$ X-ray source ($h\nu 1486\text{eV}$) generated from aluminium anode operating at the emission voltage 15keV and 5mA . The base pressure within the spectrometer during examination was 6.5×10^{-10} bar. The films of catalyst samples were prepared by dissolving a few milligrams of each sample in chloroform and methanol (3:1) then coating on the silicon wafer surface. The surfaces were exposed to near infrared light to evaporate the solvent to make a thin film. All spectra were referenced by setting the hydrocarbon C 1s peak to 285eV to compensate for residual charging effects. The Brunauer–Emmett–Teller (BET) surface area analysis, pore size and pore volume measurements were obtained according to the multipoint nitrogen adsorption-desorption method at 77.3K using Micromeritics TriStar 3000 surface analyser. The catalyst samples were degassed in a vacuum oven at 120°C for 24 hours under a vacuum of 10mmHg in order to remove any moisture and/or absorbed gases on the surface of the catalyst samples prior to analysis. The N_2 adsorption isotherms were used to calculate the BET parameters for initial TiO_2 -NPs and synthesized $\text{Ti}(\text{SO}_4)_2$ nano-catalysts; however, the desorption isotherms were used to calculate the average pore size and total pore volume for both samples using the Barrett-Joyner-Halenda (BJH) method.

The particle size, morphology and surface structure of the powder samples were studied using SU8230 Hitachi scanning electron microscopy (SEM). The sample was prepared by adding a small

amount of powder into 2ml of methanol and keeping in ultrasonic bath for 10 minutes. One drop of this suspension was then put on the SEM sample holder and placed in a zone SEM cleaner in order to remove any contaminants using of UV radiation and Ozone at 1 Pascal for 10 minutes. The Transmission electron microscopy (TEM) measurements were carried out on a FEI Tecnai TF20 FEG operated at 200kV and equipped with an energy dispersive X-ray spectroscopy (EDS, Oxford INCA) to analyse the particle size, surface morphologies, location of the elements and elemental compositions of the catalyst samples. The sample was prepared by suspending a small amount of powder sample in acetone, followed by ultra-sonication for 10 minutes. One drop of this suspension was put on a carbon coated copper grid for TEM analysis.

The thermal decomposition of TiO_2 -NPs and $\text{Ti}(\text{SO}_4)_2$ nano-catalyst was measured by Stanton Redcroft thermogravimetric analysis (TGA-TGH 1000) connected via a transfer line to a Nicolet iS10 FT-IR spectrometer to confirm the decomposition of the catalyst via gas production, in particular loss of SO_x molecules and absorbed surface species. The transfer line was kept at 170°C and the interface cell oven was maintained at 220°C . (20 ± 5) mg of sample was weighted in a $100\mu\text{l}$ platinum crucible and placed in the TGA sample holder. The system was programmed to heat up the catalyst samples from 25°C to 900°C at 10°C per minute under different purge gases, nitrogen and air separately at 30ml per minute with a constant flow rate. The system was then held at 900°C for 10 minutes before being cooled to room temperature using water jacket circulator (Julabo F32). The FT-IR spectra were taken with a minimum 36 scans performed at the average signal of infrared with 4cm^{-1} a resolution ranging 400cm^{-1} to 4000cm^{-1} and the time interval of 50 seconds between spectra. The total data collection time was 90 minutes for each sample.

2.2.3.2 Biodiesel characterization

Flash point of prepared biodiesel sample was measured by an auto ramp closed cup flash point tester (Setaflash series 3, England) equipped with a coolant block unit. At ambient temperature, 2.0 ml of biodiesel sample was manually injected into the sample cup via the filter orifice and the instrument

was set on the expected flash point temperature for the biodiesel sample. The temperature ramped at 1°C-2°C/min until the flash was captured. Moreover, the pycnometric method was used to determine the density of obtained biodiesel at 15°C. Furthermore, viscosity of prepared biodiesel was measured on a Bohlin-Gemini 150 rotary rheometer (Malvern, UK). 2ml of biodiesel fuel was placed and the data was analysed based on the Newtonian model from the Bohlin program to determine the dynamic viscosity at 40°C of the biodiesel sample [5]. Additionally, trace moisture content in biodiesel was analysed by volumetric Karl Fischer titration (Mettler Toledo-V20, Germany) [61]. The acid values and percentage of FFA were measured according to the standard method [62, 63]. Finally, the cooling behavior of prepared biodiesel was examined using optical microscopy (Olympus, Japan) equipped with a hot-stage (EHEIM professional 3, Germany) to screen the crystal nucleation/growth in biodiesel sample during cooling. The sample first heated up to 50°C at 25°C/min and held at 50°C for 5 minutes to dissolve any wax materials in the sample. The system was then cooled down to -40°C at 3°C/min and then held at each specified temperature stage for 5 minutes. Images were collected with a Pixelink camera (PL-A662, Canada) at 15 seconds intervals upon cooling. Linksys32 software was used for programming (heating and cooling) and data processing.

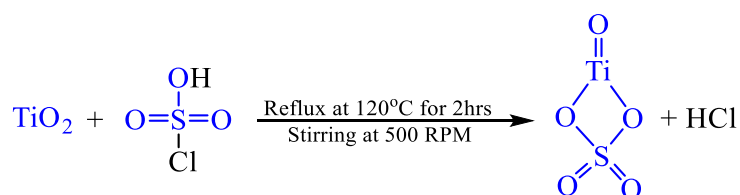
3. RESULTS AND DISCUSSION

3.1 Catalyst characterization

3.1.1 Crystal structure

TiO₂-NPs reacts with chlorosulfonic acid producing Ti(SO₄)O solid super acidic nano-catalyst (main product) and hydrochloric acid gas (by-product) as shown in proposed scheme 1. At high temperature (120°C), chlorosulfonic acid slowly generates sulphur trioxide (SO₃) and hydrochloric acid gas [64]. The by-product (HCl) gas liberated from this reaction is a corrosive gas, but in industry normally it is recovered either by neutralizing the off-gas with a very low concentration of sodium hydroxide as a basic scrubbing solution to produce sodium chloride salt or by diluting with water

[65]. The sulphur trioxide is a very aggressive electrophilic reagent that rapidly reacts with TiO₂-NPs to form TiO₂-sulfonic acid. In the presence of a reflux condenser for 2hrs, the formed TiO₂-sulfonic acid is slowly converted into the sulphated titanium oxide or oxysulfate titania [Ti(SO₄)O].



Scheme 1: Preparation of Ti(SO₄)O nano-catalyst

The XRD patterns of base TiO₂-NPs indexed using JCPDS-ICDD confirmed 81.6% of tetragonal anatase phase (04-014-5762, TiO₂) and 18.4% of tetragonal rutile phase (01-072-4815, TiO₂). The major diffraction peaks of nano-TiO₂ were observed at 2θ values of 25.30°, 36.95°, 37.80°, 38.56°, 48.03°, 53.89°, 55.06°, 62.11°, 62.69° and 68.76° assigned to the (101), (103), (004), (112), (200), (105), (211), (213), (204) and (116) reflections for the anatase structure of TiO₂, respectively. The rest of the diffraction peaks were observed at 2θ values of 27.43°, 36.07°, 39.18°, 41.23°, 44.04°, 54.31°, 56.62°, 62.75°, 64.04°, 65.50° and 68.99° corresponded to the (110), (101), (200), (111), (210), (211), (220), (002), (310), (221), (301) and (112) planes for the rutile structure of TiO₂, respectively, as shown in figure 1.

In the case of the synthesised nano-catalyst (Ti(SO₄)O), the XRD patterns indexed using JCPDS-ICDD in Figure 1 confirm that all diffraction peaks matched with titanium sulphate oxide or titanium oxysulfate (Ti(SO₄)O, 04-011-4951). It should be noted that most of the diffraction peaks were sharp peaks indicating the high crystallinity degree of the Ti(SO₄)O nano-catalyst sample. However, there are some broad peaks with low intensities at 36.80°, 45.43°, 51.89°, etc., presumably due to the amorphous degree, which could be explained by the presence of sulphate group inside the chemical structure of prepared nano-catalyst.

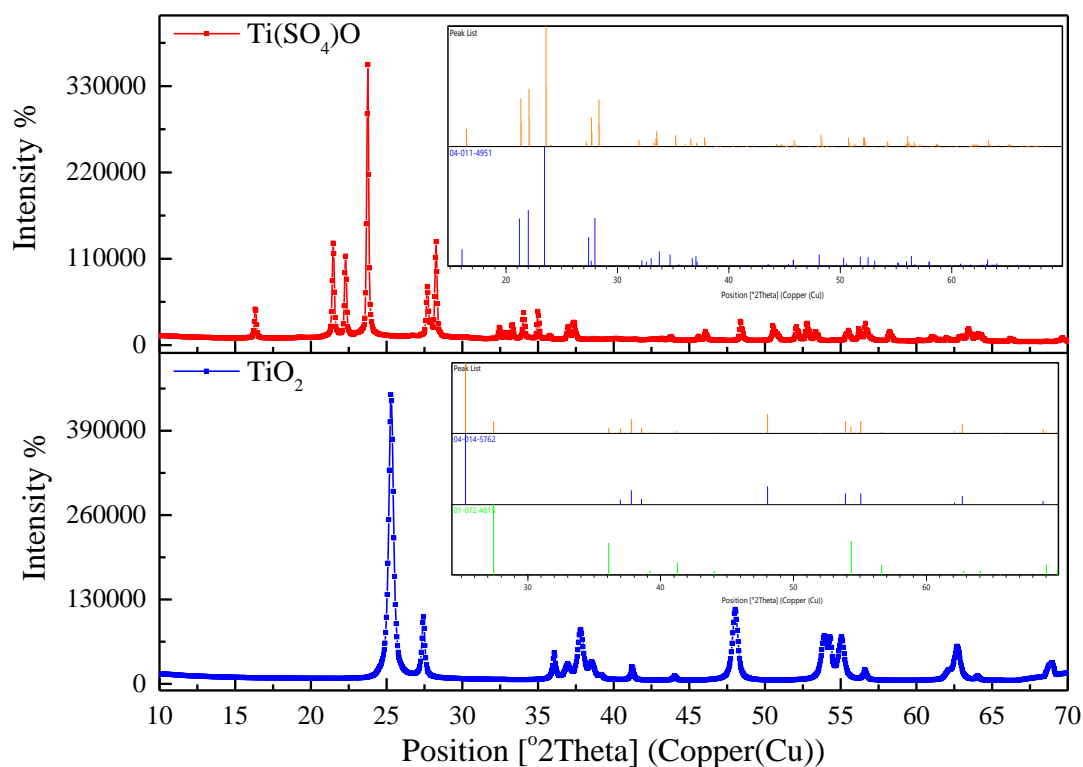


Figure 1: Powder XRD profiles for TiO₂ and Ti(SO₄)O nano-catalyst samples at room temperature.

The average particle sizes of TiO₂ and Ti(SO₄)O nano-catalysts were calculated as 28nm and 45 nm, respectively, using Debye-Scherrer's method [66-68] ($d = k\lambda/\beta\cos\theta$), where k is a shape factor of the particles, β is the full width at half maxima of the diffraction peaks (FWHM), λ is a wavelength of the CuK α radiation, and θ is the incident angle of the X-rays.

3.1.2 Surface analysis

3.1.2.1 Fourier Transform infrared (FT-IR) spectroscopy

The FT-IR spectrum of the prepared Ti(SO₄)O nano-catalyst shows five extra band vibrations than the spectrum of TiO₂-NPs, suggesting sulphate group's incorporation into the structure of the TiO₂ molecules as shown in figure 2. The sharp band in Ti(SO₄)O at 626.4cm⁻¹ and the broad band in TiO₂ at 553cm⁻¹ were assigned to the vibration stretching of Ti-O [69, 70]. Moreover, three extra strong bands at 786.9cm⁻¹, 915cm⁻¹ and 1044.7cm⁻¹ in Ti(SO₄)O nano-catalyst spectrum correspond to S-O stretching vibrations in bidentate sulphate coordinated to the Ti⁴⁺ metal [50, 71-73]. The strong band at 1216.9cm⁻¹ referred to S=O asymmetric stretching vibration whilst the other strong

band at 1132.9cm^{-1} attributed to the S=O symmetric stretching vibration. The band at 1690.1cm^{-1} in $\text{Ti}(\text{SO}_4)\text{O}$ and at 1637.8cm^{-1} in TiO_2 nano-catalyst correspond to H-O-H symmetric vibration of absorbed water molecules on the surface of both catalysts [74, 75]. The vibration bands at 2360.8cm^{-1} and 2352.5cm^{-1} in TiO_2 and $\text{Ti}(\text{SO}_4)\text{O}$ nano-catalysts spectra, respectively, could correspond to asymmetric stretching of CO_2 molecules in the air, contaminated the surface of both nano-catalysts [76]. The broad bands at 3045cm^{-1} to 3400cm^{-1} in both catalysts assign to the stretching vibration of O-H functional groups [74, 75].

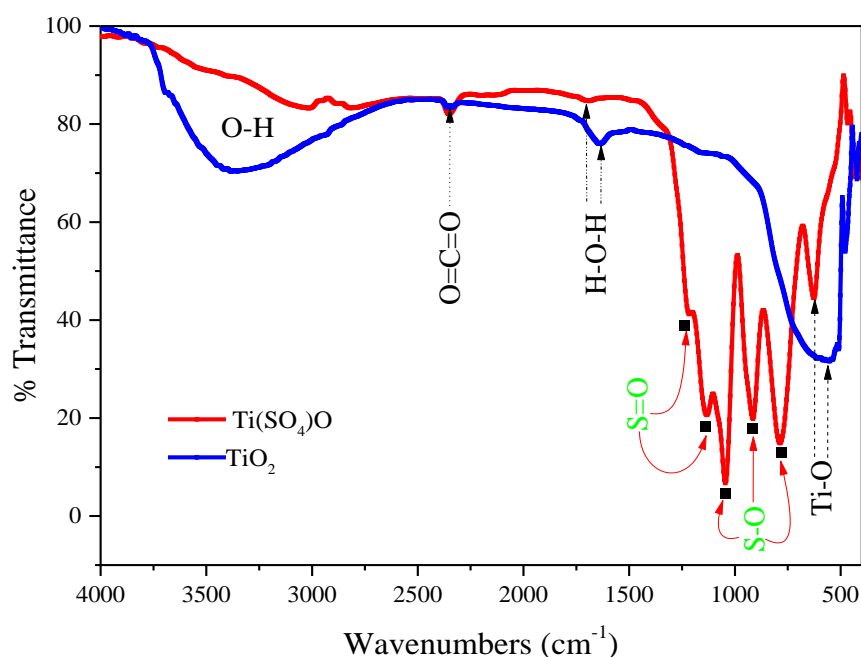


Figure 2: The FT-IR spectra of TiO_2 and prepared $\text{Ti}(\text{SO}_4)\text{O}$ nano-catalyst samples at ambient temperature. The black dots indicate the extra absorption bands for S=O and S-O in the prepared nano-catalyst.

3.1.2.2 X-ray photoelectron spectrum (XPS)

Figure 3 shows the high resolution XPS spectrum survey scan for TiO_2 and $\text{Ti}(\text{SO}_4)\text{O}$ nano-catalysts. In case of TiO_2 -NPs the catalyst contains not only Ti (464eV) and O (530 eV) elements but also some carbon observed at 285eV, presumably due to the CO_2 contamination. Whereas, in the case of synthesised $\text{Ti}(\text{SO}_4)\text{O}$ catalyst, four significant peaks were observed at 167eV, 285eV, 457.35eV,

and 529.95eV, corresponding to S 2p, C 1s, Ti 2p and O 1s, respectively. The band at 167 eV is a clear evidence of sulphate group in the synthesised nano-catalyst [Ti(SO₄)O].

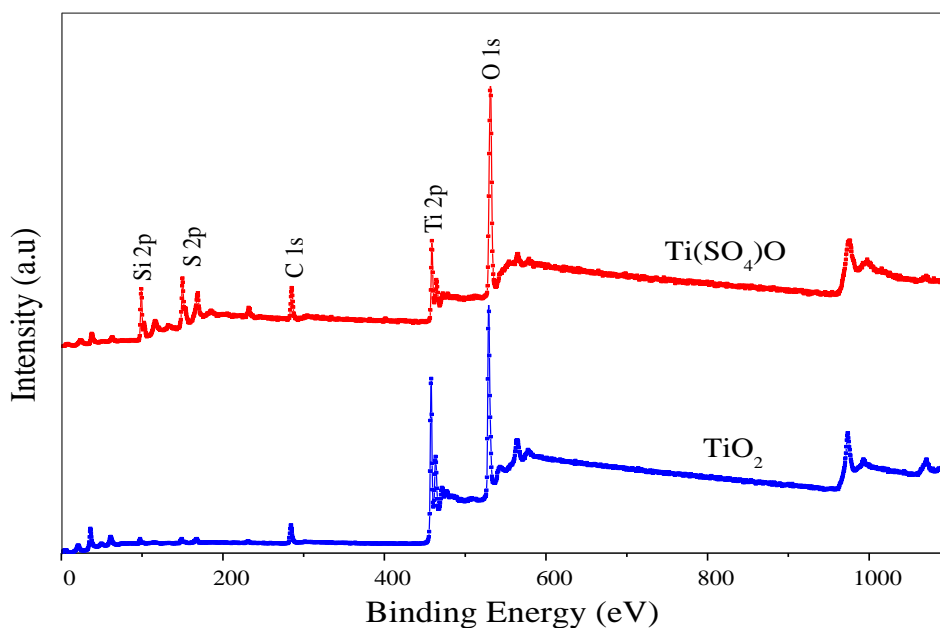


Figure 3: XPS survey scan of TiO₂ and Ti(SO₄)O nano-catalyst samples showing the chemical environments at 167eV for S 2p in the obtained nano-catalyst.

The spin-orbital splitting between Ti 2p_{3/2} (at 462.75eV) and Ti 2p_{1/2} (at 456.94eV) is 5.81eV, as shown in figure S1c (supplementary information). This is most prominent implication that titanium in the TiO₂ exists in a quadrivalent oxidation state (Ti⁴⁺) in the anatase phase of the TiO₂. Figure S1a (supplementary information) shows the deconvoluted O 1s peaks of TiO₂-NPs. The spectra yielded three Gaussian peaks. The first band located at 530.2eV with full width at half maximum (FWHM) of 1.177eV (Δ E_{BE}) could be attributed to the Ti=O from TiO₂. The second peak centered at binding energy of 531.2eV could be related to the C=O from absorbed CO₂ in air on the surface of the nano-catalyst. The last peak detected at 532.52eV is assigned to the O-H of absorbed moisture from air on the surface of the TiO₂-NPs by forming [-Ti(OH)-O-Ti-O-]. This agrees with the reported XPS in the literature for TiO₂ as listed in table S2 (supplementary information).

Based on the result presented in table S2 (supplementary information), it can be inferred that the surface of TiO₂ was very active and contaminated with CO₂ and H₂O from the air [77]. In the case

of $\text{Ti}(\text{SO}_4)\text{O}$, the O 1s spectra was fitted and resulted in two Gaussian components (figure S1b, supplementary information). A broad peak located at 530.76eV corresponds to the lattice oxygen in $\text{Ti}=\text{O}$ and $\text{S}=\text{O}$, this could be due to the binding energy of the de-convoluted O 1s peaks for $\text{Ti}=\text{O}$ and $\text{S}=\text{O}$ falling in the same region which made it difficult to distinguish between the contribution of both species [78]. The band detected at 531.72eV correlated to the two different oxygen species and this must be due to the presence of $\text{Ti}-\text{O}$ and $\text{S}-\text{O}$ bonds. Moreover, the binding energy of the Ti $2p_{3/2}$, as can be seen in figure S1d (Supplementary information), in $\text{Ti}(\text{SO}_4)\text{O}$ nano-catalyst was shifted by 2.01eV compared to the binding energy of the Ti $2p_{3/2}$ in nano-sized TiO_2 . Furthermore, the Ti $2p_{1/2}$ peak in $\text{Ti}(\text{SO}_4)\text{O}$ located at 458.7eV could be ascribed to Ti^{4+} oxidation state [79]. The binding energy of S 2p was observed at 167eV which agrees with the reported earlier values for S-O bonds in sulphate groups [80, 81]. This elucidates that one of the oxygen atoms in the TiO_2 nano-catalyst was replaced by sulphate group as in obtain nano-sized $\text{Ti}(\text{SO}_4)\text{O}$ catalyst.

The detailed comparison of the elemental compositions using TEM-EDS analysis and relative surface elemental composition using XPS analysis for TiO_2 and $\text{Ti}(\text{SO}_4)\text{O}$ nano-catalyst samples are presented in table 2.

Table 2 Compared atomic ratios for TiO_2 and $\text{Ti}(\text{SO}_4)\text{O}$ nano-catalysts using XPS and TEM-EDS analyses

	Bulk atomic ratio % determined by TEM-EDS analysis		Surface atomic ratio% determined by XPS analysis	
	O/Ti	S/Ti	O/Ti	S/Ti
TiO_2	1.55:1±0.005	---	2.35:1±0.008	---
$\text{Ti}(\text{SO}_4)\text{O}$	4.45:1±0.006	0.74:1±0.002	4.80:1±0.005	1.00:1±0.078

The atomic ratio of O/Ti in TiO_2 -NPs measured by TEM-EDS was 1.55:1±0.005 whilst this ratio was 2.35:1±0.008 by XPS. This could be due to the surface of the nano-catalyst being contaminated with CO_2 and H_2O in air which is confirmed by FT-IR and presence of sp^2 hybridized carbon in XPS

survey scan spectrum at 285eV. The ratio of S/Ti and O/Ti in Ti(SO₄)O nano-catalyst have also been calculated from TEM-EDS and XPS analyses. According to both analyses the atomic ratio of S/Ti was around 1:1 and for O/Ti was 5:1. Based on this result, it can be conclude that there was only one oxygen in TiO₂ is replaced by sulphate group. This result is consistent with XRD analysis of Ti(SO₄)O.

3.1.2.3 Brunauer–Emmett–Teller (BET) surface area

In general, surface area plays a key role in effectively enhancing the activity of solid acid catalysts for esterification and transesterification processes as large surface area facilitates the reactant molecules access to the acid sites on the solid catalyst surface. The nitrogen adsorption isotherms were used to calculate the BET surface area for both samples whilst the desorption isotherms were used to calculate the average pore size and total pore volume for both samples using the Barrett-Joyner-Halenda (BJH) method. The detailed BET, average pore size and total pore volume of TiO₂ and Ti(SO₄)O nano-catalyst samples are summarised in Table 3. Based on these results, the loading of sulphate groups on TiO₂ has resulted in relatively lower BET surface area as compared to the TiO₂; this may be explained by the aggregation of the very small crystallites in synthesized nano-catalyst with their low ordering and crystallinity (see figure 7a). It was also found that the average pore size and total pore volume of Ti(SO₄)O nano-catalyst increased compared to TiO₂ nanoparticles. This might be due to the effect of sulphate group which is incorporated into the TiO₂ structure and could perhaps account for the increase in the concentration of the structural disorder and reduction of surface area in the prepared nano-catalyst.

Table 3 Summary of the properties of TiO₂ and Ti(SO₄)O nano-catalysts

Type of catalyst	BET surface area (m ² /g)	BJH mean pore size (nm)	BJH total pore volume (cm ³ /g)
TiO ₂	48.6398	12.8722	0.156571
Ti(SO ₄)O	44.4563	22.7347	0.312459

The nitrogen adsorption-desorption isotherms of TiO₂ and Ti(SO₄)O nano-catalysts could be classified as type IV with one hysteresis loops at a relative pressure range of 0.75-1.0 as depicted in figure 4. The experimental results clearly confirmed that both samples are mesoporous with the type of hysteresis loops H1 according to the IUPAC classification witnessed for uniform pore sizes due to differences in absorption and desorption [82]. In the case of Ti(SO₄)O, nevertheless, the pore size distribution is broader compared to TiO₂ NPs sample which is more preferable for minimizing diffusion limitations for long alkyl chain hydrocarbons in FFA/triglyceride (TG) [83]. It is also believed that the prepared Ti(SO₄)O possesses some interesting characteristics such as mixed large particles with very fine particles, large and accessible pore surfaces, specifically useful for photocatalysis.

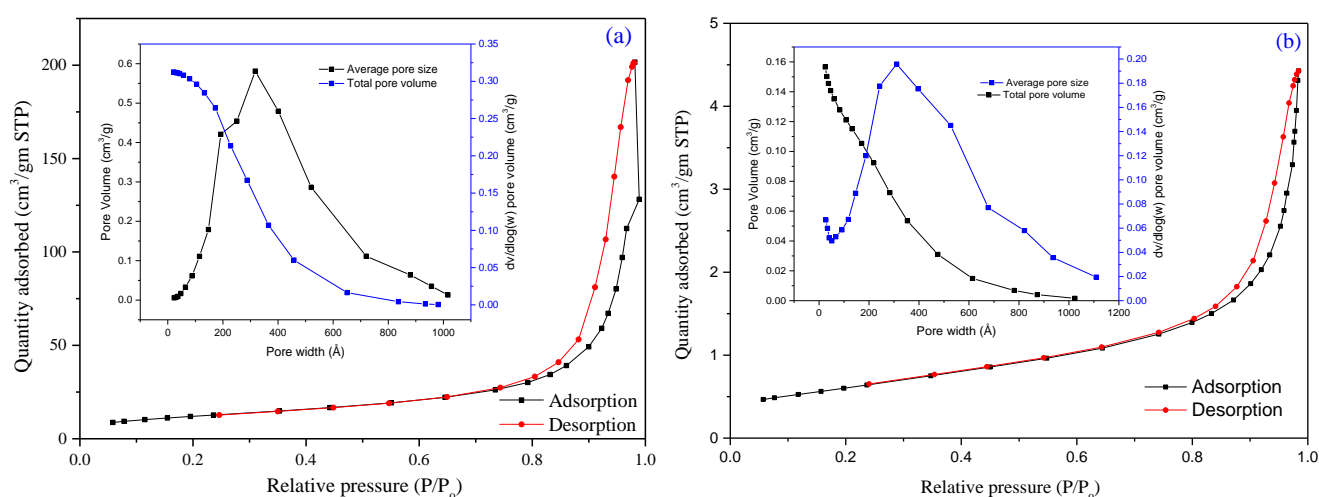


Figure 4: N₂ adsorption-desorption isotherms and total pore volumes for (a) Ti(SO₄)O and (b)TiO₂ nano-catalysts.

3.1.2.4 Morphology of the nano-sized catalysts

Figure 5 (a) and (b) shows the SEM images of TiO_2 and $\text{Ti}(\text{SO}_4)\text{O}$ samples, respectively, at 100K magnification. It can be seen that TiO_2 -NPs (Figure 5a) have relatively uniform size particles with some agglomerates, whereas titanium sulphate oxide nano-catalyst (Figure 5b) has completely different particle size distribution.

High resolution TEM (HRTEM) clearly confirmed the actual size of the particles, crystallographic phases and morphologies as depicted in Figure 6 (a) and (b) for TiO_2 and $\text{Ti}(\text{SO}_4)\text{O}$ nano-catalyst samples, respectively. It can be observed that the $\text{Ti}(\text{SO}_4)\text{O}$ particles aggregate to each other forming a network, possibly due to the electrostatic attraction among SO_4^{2-} species.

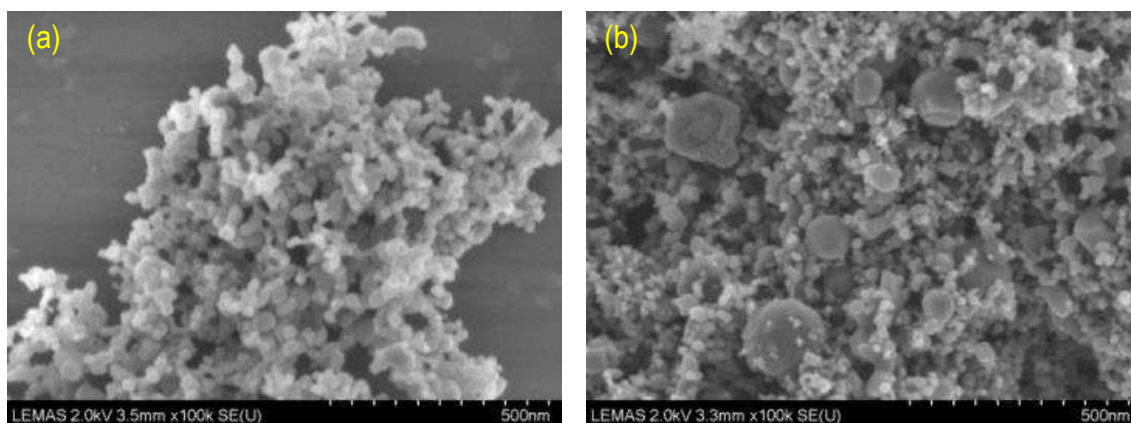


Figure 5: SEM micrograph images of (a) TiO_2 and (b) $\text{Ti}(\text{SO}_4)\text{O}$ nano-catalyst samples, in case of $\text{Ti}(\text{SO}_4)\text{O}$ showing the presence of different size of particles.

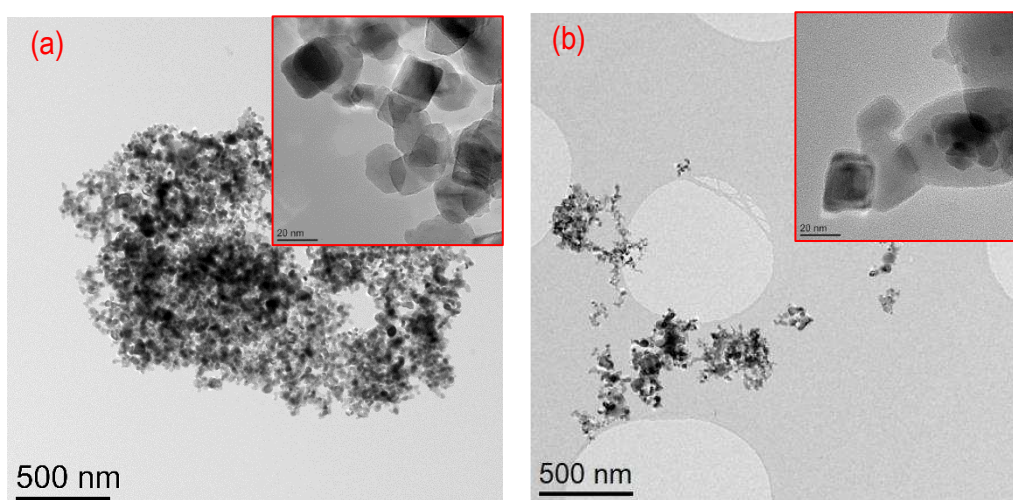


Figure 6: TEM images of (a) TiO_2 showing uniform size of particles having irregular morphology and (b) $\text{Ti}(\text{SO}_4)\text{O}$ nano-catalyst showing the presence of mixed large particles with very fine particles.

The number based particle size distributions of TiO_2 and $\text{Ti}(\text{SO}_4)\text{O}$ nano-catalysts are presented as histograms in figure S2 (supplementary information). The synthesised $\text{Ti}(\text{SO}_4)\text{O}$ were non-uniformly distributed and with an average particle size diameter of ~ 25 nm (as per 108 particles in different TEM images). In contrast, the particles of TiO_2 -NPs were less scattered with an average particle size diameter of ~ 22.34 nm which is in agreement with the data from supplier. It is also noticeable from TEM images that most TiO_2 -NPs have tetragonal or hexagonal morphologies.

HRTEM image confirms polycrystalline TiO_2 particles as depicted in figure 7a. The visible lattice fringes (figure 7a) with interplanar spacing of 3.518\AA correspond to (101) lattice planes of TiO_2 according to JCPDS-ICDD file 04-014-5762. HRTEM image proves that prepared $\text{Ti}(\text{SO}_4)\text{O}$ nano-catalyst contains a small fraction of polymorphous as depicted in figure 7. It was also found that these results are in agreement with XRD result for $\text{Ti}(\text{SO}_4)\text{O}$ nano-catalyst (see figure 1). The lattice fringes (figure 7c) with interplanar spacing of 3.078\AA correspond to (301) lattice planes of $\text{Ti}(\text{SO}_4)\text{O}$ (JCPDS-ICDD 04-011-4951). This was further confirmed by the selected area electron diffraction (SAED) pattern of the TiO_2 -NPs sample showing a set of diffused spot rings, as shown in figure 7(b), whilst the SAED pattern of $\text{Ti}(\text{SO}_4)\text{O}$ nano-catalyst shows brightness and spotty rings are shown in figure 7(d).

The details of studies of the d-spacing values calculated from SAED spotty rings with the reported d-spacing values for TiO_2 and $\text{Ti}(\text{SO}_4)\text{O}$ in the JCPDS-ICDD card numbers 04-014-5762 (Anatase, TiO_2), 01-072-4815 (Rutile, TiO_2) and 04-011-4951 ($\text{Ti}(\text{SO}_4)\text{O}$) are presented in table S3 (supplementary information). It is noteworthy that the results of ICDD agree with d-spacing values obtained from XRD and SAED in this investigation. These results further confirm the successful synthesis of $\text{Ti}(\text{SO}_4)\text{O}$ nano-catalyst using TiO_2 -NPs and chlorosulfonic acid as a reagent.

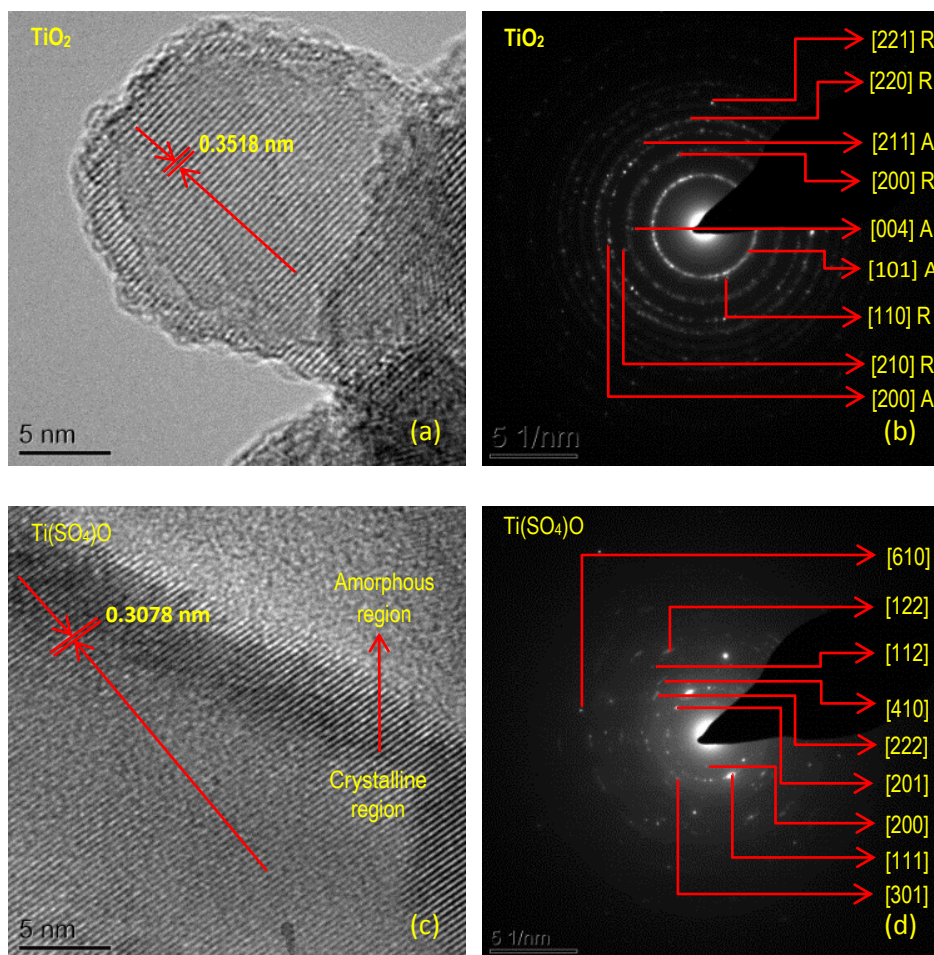


Figure 7: Images of HRTEM for (a) TiO_2 confirmed the 101 lattice planes and (c) prepared $\text{Ti}(\text{SO}_4)\text{O}$ confirmed the 301 lattice planes; whilst images of (b and d) showing the SAED patterns for TiO_2 and $\text{Ti}(\text{SO}_4)\text{O}$, respectively.

TEM-EDS analysis of prepared $\text{Ti}(\text{SO}_4)\text{O}$ nano-catalyst showed an extra strong peak on the EDS graph at 2.15keV (Figure S3, supplementary information), corresponding to the sulphur element. In both TEM-EDS graphs, extra peaks of C and Cu were observed due to the carbon-coated copper TEM grids used during analysis of the samples as shown in figure S3. Furthermore, the ratio of the intensities of titanium signal to sulphur signal was around 1:1wt% at several different whole captured areas in TEM images for the synthesised $\text{Ti}(\text{SO}_4)\text{O}$. The presence of a large amount of sulphur spread over the entire area of the prepared nano-catalyst has been further verified by TEM-mapping analysis (figure 3c, supplementary information). These findings provide direct evidence that sulphur, titanium and oxygen are the main elements present in the prepared nano-catalyst. Meanwhile,

titanium and oxygen are the only elements present in the raw material nano-catalyst (TiO₂-NPs), except cu and c from TEM grids (see figure S3a, supplementary information).

3.1.2.5 Stability analysis

TGA was carried out to identify the thermal and oxidation stability of the nano-catalyst samples during heating from 25°C to 900°C. Figure 8 reveals the stability of Ti(SO₄)O and TiO₂ samples in nitrogen (thermal) and air (oxidative). The TGA curve of Ti(SO₄)O displayed a small weight loss at 50°C to 200°C, indicating the desorption of water molecules from the surface of the nano-catalyst (see figure 8a). One can see that Ti(SO₄)O sample has an almost negligible weight loss up to 600°C heating in both air and N₂ purge gases. These results clearly indicate that the sulphate groups are fairly stable in the structure of the prepared nano-catalyst. The results also showed significant weight loss (about 47%) at 600°C to 800°C. In contrast, there is no further mass loss up to 900°C. This might be due to the degradation of sulphate groups in the Ti(SO₄)O nano-catalyst sample, as can be described by the following equations:

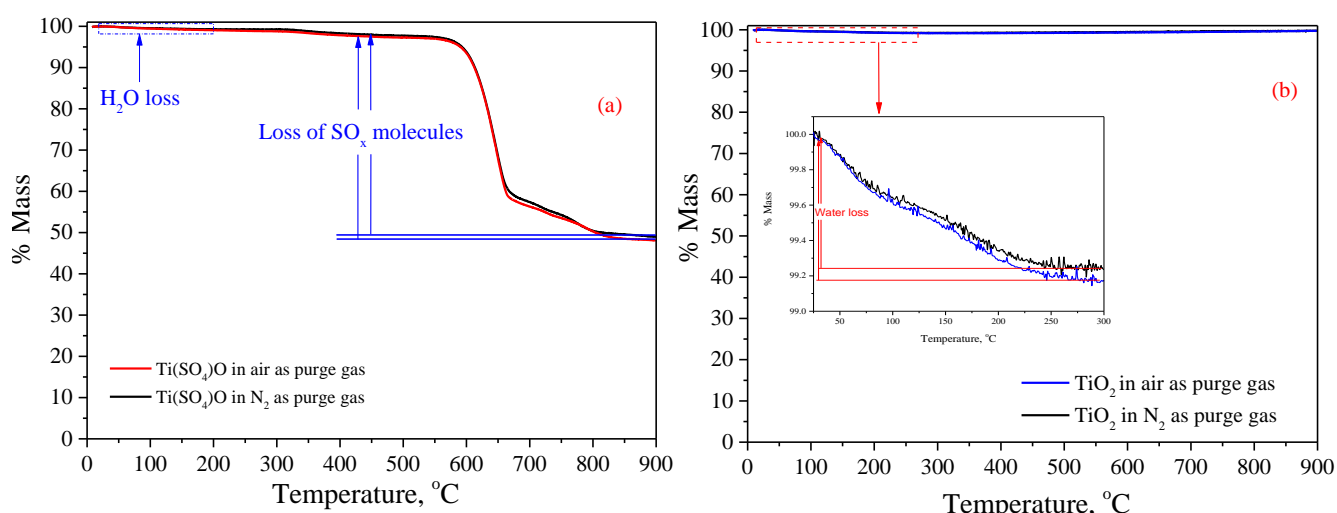
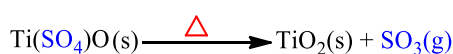


Figure 8: TGA profiles of (a) Ti(SO₄)O and (b) TiO₂ nano-catalyst samples.

On the other hand, the mass loss of the unmodified TiO₂ nano-particle (see figure 8b) shows that there was only one stage of weight loss from ambient temperature to 220°C, due to the desorption of H₂O molecules from the surface of TiO₂ nano-particles, evidence of which was observed also in absorption peaks in FT-IR spectrum at 1690.1cm⁻¹ and 3400cm⁻¹ (see figure 2). It can be noticed also that the stability of the nano-catalysts in nitrogen as a purge gas (inert) and air as a purge gas (oxidiser) show similar behaviour.

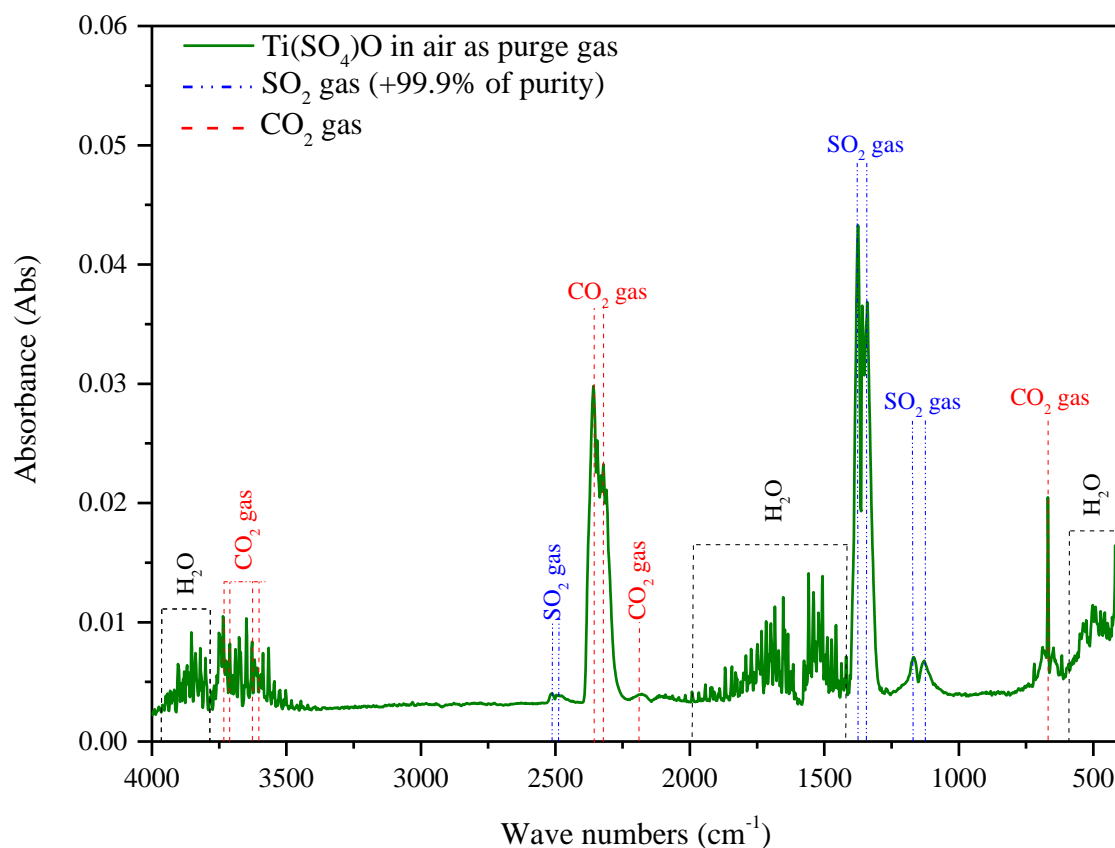


Figure 9: 2D representation of FT-IR spectrum for evolved gaseous from Ti(SO₄)O

The 2D representation of output FT-IR spectrum for evolved gases from the TGA-FTIR analysis for Ti(SO₄)O are presented in figure 9. It can be observed that the main evolved gases have been identified as SO₂-loose, CO₂-loose, and H₂O-loose through spectral interpretation and comparison with database reference spectra for pure SO₂ and CO₂. In Grand-Schmidt thermographs for Ti(SO₄)O nano-catalyst, four regions with intense peaks are observed which are: (i) bands between (3800cm⁻¹-3900cm⁻¹) and (1500cm⁻¹-1700cm⁻¹) due to O-H vibration bands from H-O-H molecule that is

always present when the sample is sensitive to moisture; (ii) peaks between 3580cm^{-1} - 3780cm^{-1} and at (2250cm^{-1} - 2400cm^{-1}) as well as at around (600cm^{-1} - 720cm^{-1}) are related to $\text{O}=\text{C}=\text{O}$ vibration bands contaminated CO_2 from atmosphere; (iii) bands between (1080cm^{-1} - 1400cm^{-1}) and at region (2460cm^{-1} - 2052cm^{-1}) due to $\text{O}=\text{S}=\text{O}$ vibration bands from decomposition of the nano-catalyst; and (iv) peaks showed at low wavenumber (400cm^{-1} - 580cm^{-1}) attributed to an intermolecular bond bending vibrations which are usually not taken into account. It should also be noted that there was no hydrogen sulfide gas detected during the pyrolysis of this nano-catalyst, confirming that there was no sulfonic acid attached on the surface of TiO_2 -NPs.

In the case of TiO_2 NPs, there were only CO_2 and H_2O species released at various time periods. The amount of CO_2 and SO_2 evolved species versus time of TiO_2 and $\text{Ti}(\text{SO}_4)\text{O}$ nano-catalysts in air and N_2 as purge gases during pyrolysis are shown in figure 10 (a & b).

In both samples the wavenumber ranges (2150cm^{-1} to 2400cm^{-1}) and (1250cm^{-1} to 1400cm^{-1}) were chosen to process the chemigram profiles of CO_2 gaseous and SO_2 gaseous in both nano-catalysts, respectively. The analysis of CO_2 chemigram profiles showed negligible amounts of CO_2 gases are released from the pyrolysis of both nano-catalysts; whereas, the surface of $\text{Ti}(\text{SO}_4)\text{O}$ nano-catalyst seen possessed a higher value of contaminated CO_2 gases as compared to the surface of TiO_2 NPs, (see figure 10a). Meanwhile, the evolved SO_2 gaseous (as shown in figure 10b) in the decomposition of $\text{Ti}(\text{SO}_4)\text{O}$ nano-catalyst started after 54 minutes of the pyrolysis process with high concentration then the width of the peak increased with time up to the end of pyrolysis. These results further confirms that sulphate group has been incorporated into the structure of TiO_2 -NPs for $\text{Ti}(\text{SO}_4)\text{O}$.

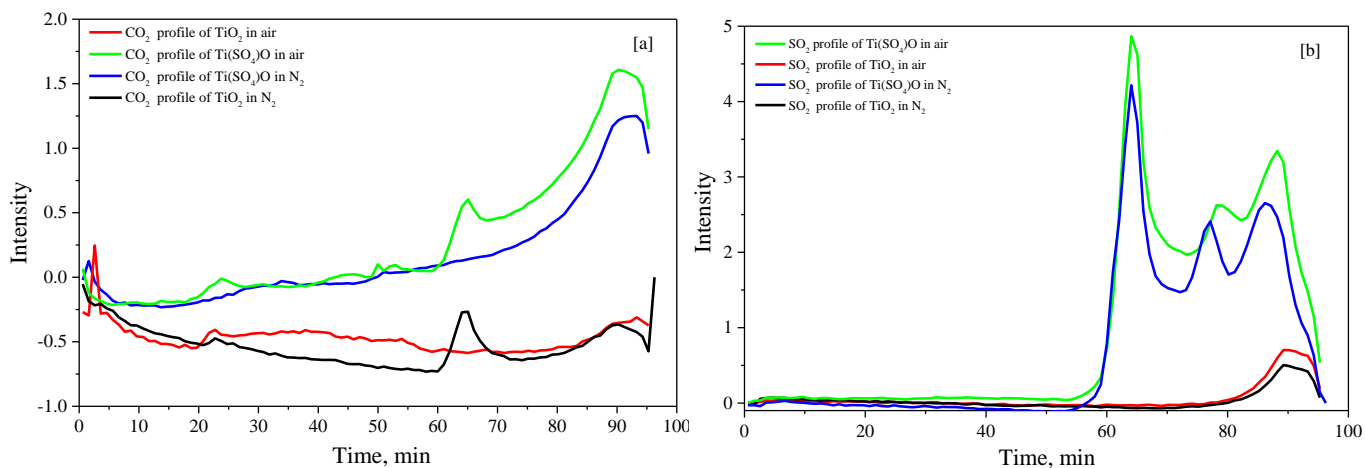


Figure 10: Chemigram profiles of (a) CO₂ (b) SO₂ species released from TiO₂ (b) Ti(SO₄)O nano-catalyst samples

3.2 Catalytic performance

The FAME yield was investigated under different catalytic process parameters including methanol to UCO mole ratio, reaction temperature, catalyst loading, and time of esterification/transesterification, see figure 11, in order to establish the optimum reaction conditions for the esterification/transesterification process of UCO to biodiesel. The esterification/transesterification of UCO with methanol using Ti(SO₄)O as a solid acid catalyst is a liquid-liquid-solid reaction (three phase system) at which the mass transfer rate of reactant molecules between the UCO-methanol-catalyst phases is very slow. The conversion rate is normally found to increase with reaction time due to an increase in the miscibility of the UCO into methanol [84, 85].

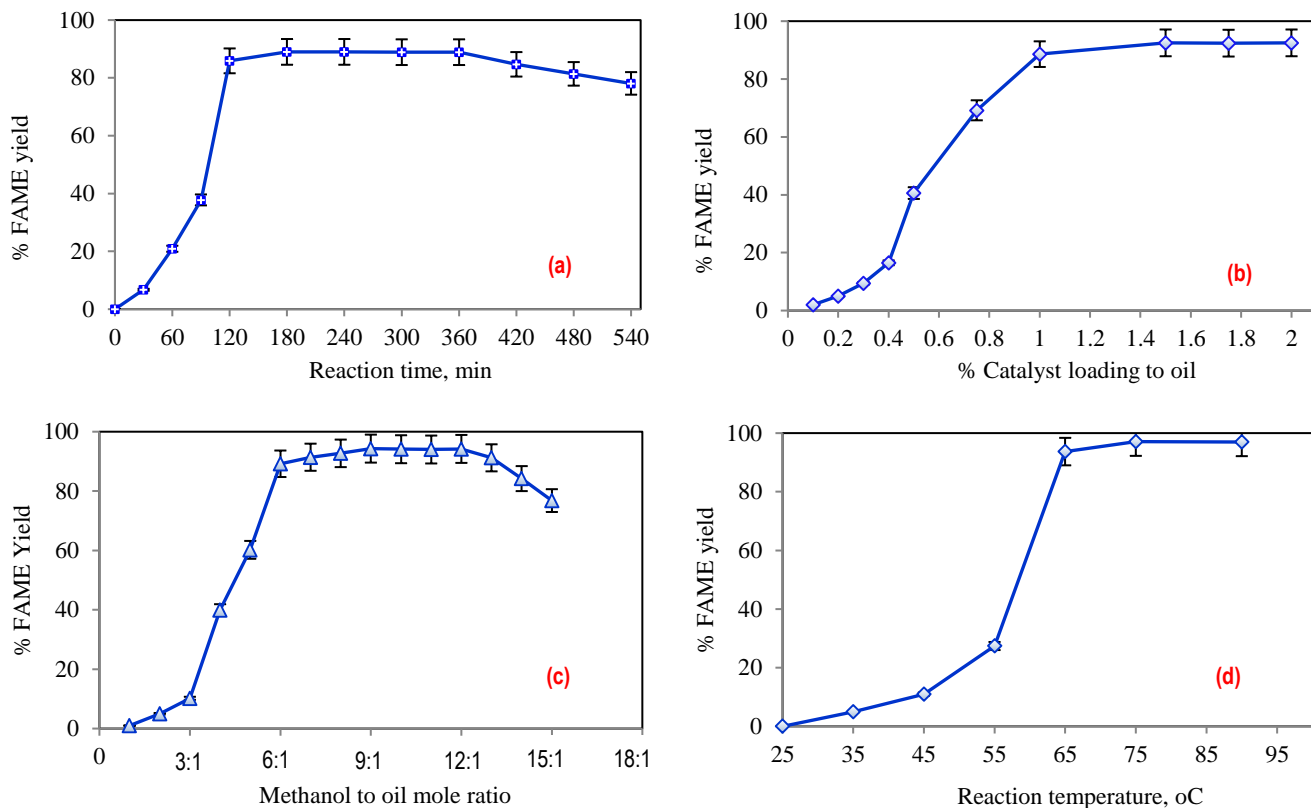


Figure 11: The effects of (a) reaction time, (b) $\text{Ti}(\text{SO}_4)_2\text{O}$ nano-catalyst loading to UCO, (c) mole ratio of methanol to UCO, and (d) reaction temperature on the percentage of FAME yield.

The reaction time was varied between 30 to 540 minutes, while keeping other reaction process parameters constant at 1.0 mass% of $\text{Ti}(\text{SO}_4)_2\text{O}$ catalyst loading to UCO, 6:1 molar ratio of methanol to UCO, 65°C reaction temperature, 600RPM agitation rate, 0.14% moisture content, and 2.034 mass% free fatty acid contents in feedstock. It can be noted that the increase of reaction time from 30 minutes to 3 hours led to the enhancement of FAME yield to 89% as shown in Figure 11(a). This can be explained by the rate constants for mono-glycerides and di-glycerides conversion to glycerol and mono-glycerides being very low compared to triglycerides [86]. Additionally, a longer reaction time (after 6 hours) resulted in slowly reduced production yield, possibly due to increasing the probability of pushing the reverse reaction. Similar results has been reported by Nayebzadeh [29] where a further increase in esterification reaction time resulted in a production yield decrease.

The optimum ratio of $\text{Ti}(\text{SO}_4)_2\text{O}$ catalyst loading was determined under the other fixed reaction conditions, i.e. at 3hrs reaction time, 6:1 molar ratio of methanol to UCO, 65°C reaction temperature,

600RPM agitation rate, 0.14% moisture content, and 2.034 mass% free fatty acid. Figure 11(b) depicts that 1.5% of $\text{Ti}(\text{SO}_4)_2$ was the optimum amount in achieving the highest production yield of 92.5% under aforementioned reaction conditions. This is due to the fact that increasing the catalyst concentration in the system leads to an increase in the total number of active sites which results in a faster reaction rate to reach reaction equilibrium [87].

The stoichiometric ratio for transesterification reaction, theoretically, requires three moles of methanol per mole of TG but esterification reaction requires one mole of methanol per mole of FFA. However, the transesterification process experimentally requires an excess of methanol in order to push the equilibrium reaction forward direction of methyl esters as the transesterification process is a reversible reaction [88]. Maximum conversion of triglycerides into FAME is ensured by the use of excess methanol due to esterification/transesterification being a reversible reaction. Figure 11(c) shows the effect of various mole ratios of methanol to UCO under the other fixed reaction process at 3hrs reaction time, 1.5 mass% $\text{Ti}(\text{SO}_4)_2$ catalyst loading to oil, 65°C reaction temperature, 600RPM agitation rate, 0.14% moisture content, and 2.034 mass% FFA contents. The highest yield of 94.3% was achieved at 9:1 mole ratio of methanol to UCO. It can be noted that an increase in methanol to UCO from 1:1 to 3:1 resulted in a slight effect on the FAME yield, while further excess of methanol from 4:1 to 9:1 increased the production yield up to the highest FAME yield. Afterwards, there was a decline in the production yield with higher mole ratios higher than 12:1. This can be explained by an additional amount of methanol helping to drive the reversible side of reaction to re-form mono-glyceride with di-glyceride and the solubility of the by-product could also be increased in the solution. In addition, water (by-product) is obtained during the esterification of FFAs in UCO feedstock lowers the activity of the catalyst.

The rate of esterification/transesterification reaction is highly affected by the reaction temperature according to Arrhenius's equation. A higher temperature also reduces the viscosities of the oils, thereby increasing the rate of the reaction. The esterification/transesterification reaction can occur at

different temperatures depending on the fatty acid profiles of raw sample oils and the type of catalyst. The effect of temperature on the FAME yield using $\text{Ti}(\text{SO}_4)_2$ as a solid acid catalyst was examined by varying the reaction temperatures from 25°C to 90°C while other process parameters were kept constant at 3hrs reaction time, 1.5 mass% $\text{Ti}(\text{SO}_4)_2$ catalyst loading, 9:1 molar ratio of methanol to UCO, 600RPM agitation rate, 0.14% moisture content, and 2.034 mass% free fatty acid content. It was found that the yield consistently increased at higher reaction temperature as shown in Figure 11(d). This can be explained by the fact that esterification/transesterification is an equilibrium process and at 25°C reaction temperature energy was not enough to break down the ester bond in the TG molecules, whilst increase of the reaction temperatures to 55°C improves the FAME yield by 27.4%. A further increase of reaction temperature significantly enhanced the production yield by 66.3% possibly due to the fact that the reaction temperature at 65°C generates more nucleophilic sites in the system. Therefore with a temperature slightly higher than the boiling point of methanol, the nucleophilic attack on the carboxylic/carbonyl groups in FFA/TG are further increased. Moreover, the highest yield of FAME (97.1%) was produced at 75°C, due to the acceleration of the mass transfer rate between the UCO-methanol-catalyst phases; higher temperature helps the activation of carboxylic/carbonyl groups in FFA/TG by protonation and the methanol nucleophilic attack on the carboxylic/carbonyl groups [89]. In this work the optimum reaction temperature was found to be lower than previous work, most probably due to the high acidity of the catalysts leading to higher activity during the reaction. Further investigations on the kinetics of this reaction could be carried out and reported in future publications.

The presence of FFA in the feedstock has a great influence on the poisoning of solid acid catalysts due to the formation of water from the esterification process[88]. Oleic acid was added to virgin oil to assess the effect of FFA on the catalytic activity of $\text{Ti}(\text{SO}_4)_2$ as solid acid nano-catalyst. The amount of FFA in oil was varied from 0.5 to 7% whilst the other parameters were set constant at optimized conditions using 3.0hrs reaction time, 1.5 mass% $\text{Ti}(\text{SO}_4)_2$ nano-catalyst loading, 9:1

molar ratio of methanol to oil, 75°C reaction temperature, 600RPM agitation rate, and 0.14% moisture content.

Table 4: The effect of FFA in feedstock on the percentage of FAME yield

Oleic acid to oil, wt %	0.5%	1%	2%	3%	4%	5%	5.5%	6%	6.5%	7%
FAME yield %	97.1	97	97.1	97.01	96.14	95.69	93.42	91.37	75.39	64.5

Noticeable from table 4, there was a slight decrease of yield up to 6.0wt% FFAs in oil, then there was a significant decrease after 6wt%, probably as the rapid esterification of oleic acid promotes the reverse methanolysis reaction of FAME and glycerol which demotes the transesterification process[90]. For that reason the esterification/transesterification reaction could be carried out at higher temperature and shorter time for raw materials containing high amount of FFA to in order to achieve maximum yield of FAME [88, 89, 91]. The investigation of the effect of high temperature on the yield of raw materials containing high FFA could be the subject of future studies.

The reusability of $Ti(SO_4)_O$ solid acid nano-catalyst was also investigated to determine the nano-catalyst life time as it can help reducing the production cost for industrial purposes. It was found that the $Ti(SO_4)_O$ can be re-used up to 8 cycles with a slight drop in catalytic activity (Figure 12) for the esterification/transesterification reactions using the optimised parametric processes conditions (3hrs reaction time, 1.5 mass% $Ti(SO_4)_O$ loading , 9:1 molar ratio of methanol to UCO, 75°C reaction temperature, 600RPM agitation rate, 0.14% moisture content, and 2.034 mass% FFA contents).

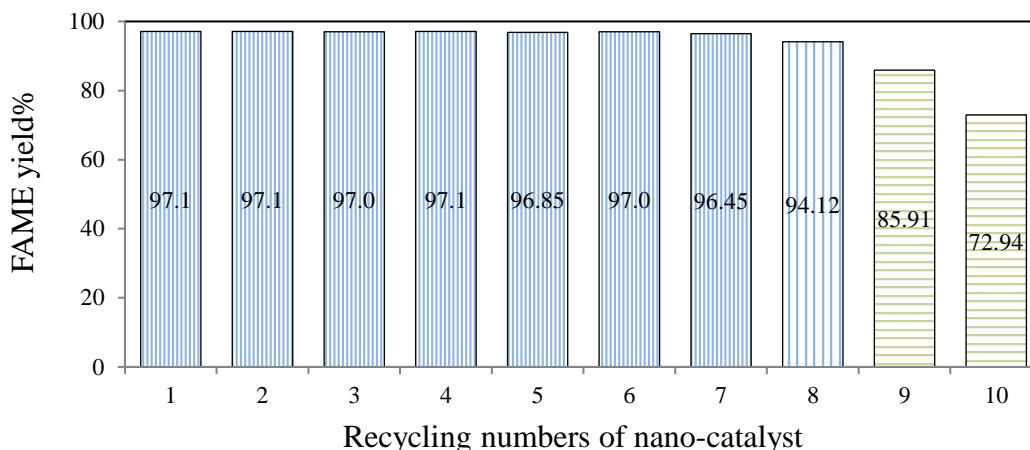


Figure 12: The effect of reusability of $\text{Ti}(\text{SO}_4)_2\text{O}$ nano-catalyst on the percentage of FAME yield.

The results revealed that the FAME yield significantly decreased for 9 and 10 trials by 11.19% and 24.16%, respectively (see Figure 12); this could be probably due to the blockage of active centres of catalyst by triglyceride (TG)/product or catalyst leaching [12, 92]. The powder XRD experiments were carried out for the recycled nano-catalyst after each run in order to investigate the catalytic deactivation. The result showed that $\text{Ti}(\text{SO}_4)_2\text{O}$ solid acid nano-catalyst maintained its structure after 8 runs as shown in Figures 13 and 14. The XRD patterns of recycled $\text{Ti}(\text{SO}_4)_2\text{O}$ from run 1 to run 7 shows that there was no loss of SO_4^{2-} groups or formation of any new phases as shown in Figure 13. This is an indication of the stability of the sulfate group in $\text{Ti}(\text{SO}_4)_2\text{O}$ nano-catalyst and durability for the first 7 cycles in simultaneous esterification and transesterification of UCO into biodiesel.

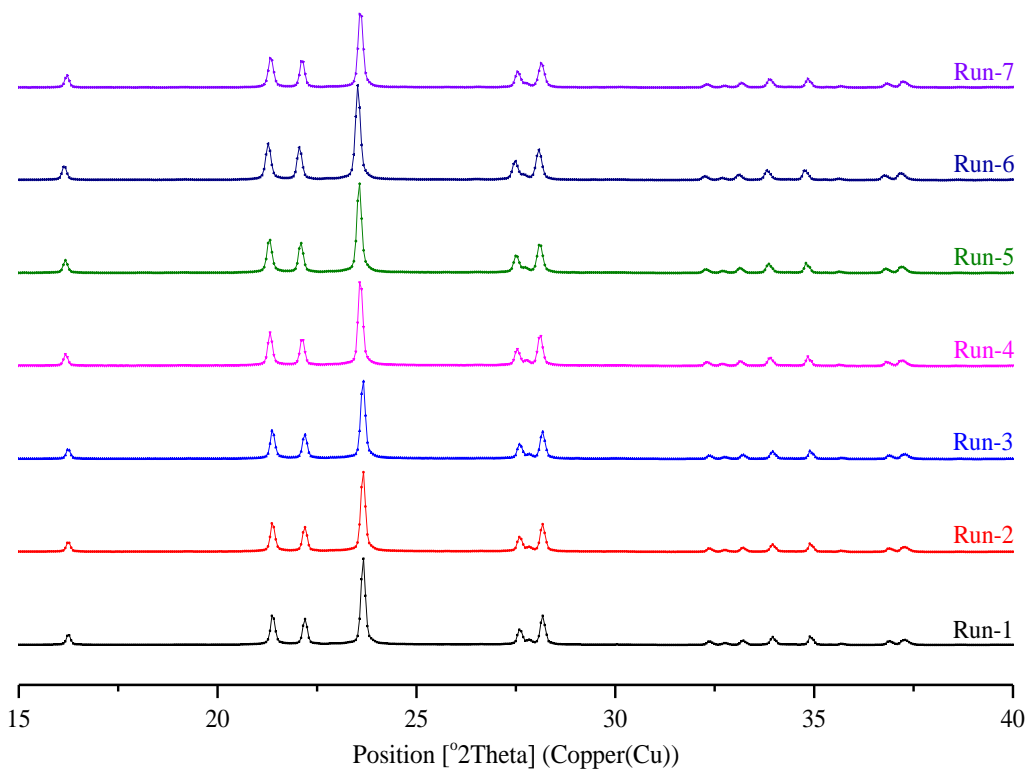


Figure 13: The powder XRD patterns of re-used $\text{Ti}(\text{SO}_4)_\text{O}$ nano-catalyst for run 1 to run 7.

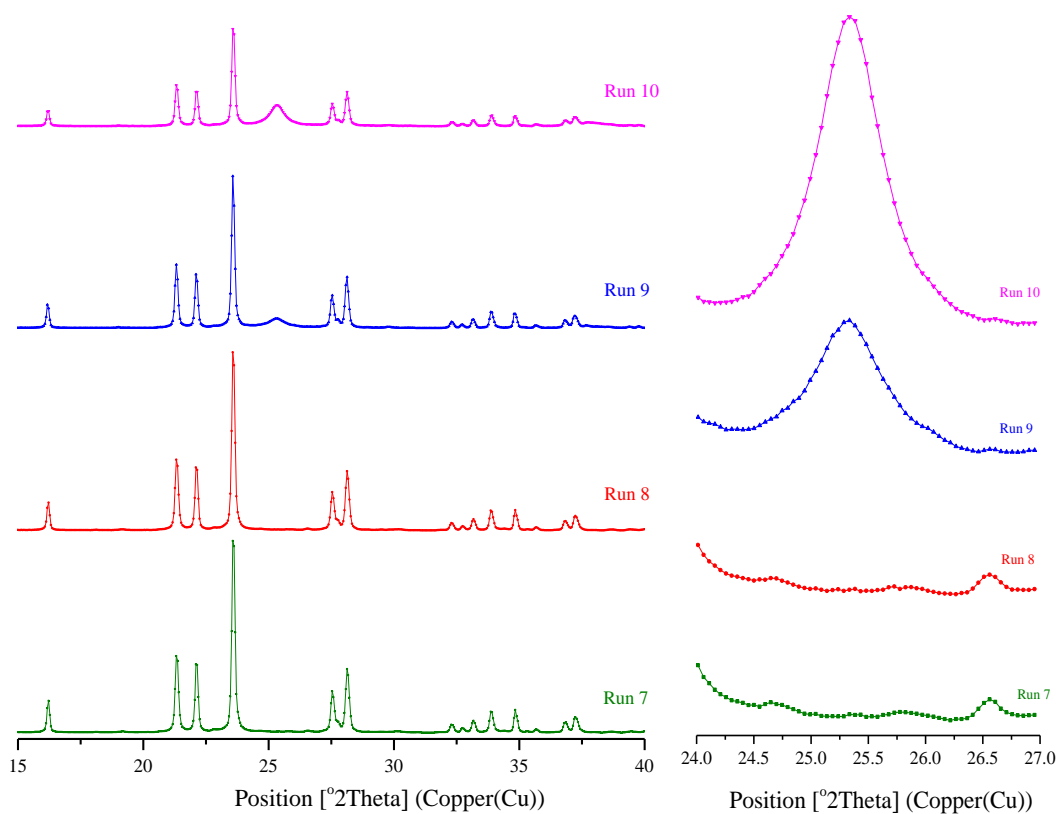


Figure 14: The powder XRD patterns of reused $\text{Ti}(\text{SO}_4)_\text{O}$ nano-catalyst from run 7 to run 10.

Figure 14 shows formation of diffraction peak at 2θ value of 25.32° assigned to the (101) reflection for the anatase structure of TiO_2 and increase of its intensity with continued re-use of the nano-catalyst beyond 8 runs (9% and 34.7% of anatase phase after 9 and 10 runs, respectively). The decrease in acidity of $\text{Ti}(\text{SO}_4)\text{O}$ nano-catalyst loss of SO_4^{2-} species might affect the esterification of FFA in UCO feedstock. In contrast, some researchers reported that leaching of SO_4^{2-} species was not the main cause for the decline in the catalytic activation of different sulfonated catalysts [93, 94]. However; in this work catalyst has a different structure than the sulphated metal oxide and XRD results confirmed that the catalytic deactivation of prepared solid acid nano-catalyst is caused by leaching of SO_4^{2-} species (see Figure 14). The regeneration of the $\text{Ti}(\text{SO}_4)\text{O}$ solid acid nano-catalyst and the performance of the regenerated nano-catalyst for simultaneous esterification and transesterification of UCO would be the subject of future studies.

3.3 Biodiesel characterizations

The biodiesel produced in the esterification/transesterification processes from UCO was characterized according to ASTM and EN standards. These results are summarised in Table 5. It can be noted that the produced biodiesel is in the range of acceptable standard specifications of biodiesel.

Table 5 Properties of biodiesel produced from UCO over $\text{Ti}(\text{SO}_4)\text{O}$ nano-catalyst

Property	Unit	Limits		Synthesised biodiesel
		ASTM D6751	EN14214	
Flash point	$^\circ\text{C}$	93 min	101 min	155
Kinematic viscosity	mm^2/s	1.9-6.0	3.5-5.0	4.58
FAME content	% mass	---	96.5 min	97.1
Acid number	mgKOH/g	0.8 max	0.5 max	0.32
Density at 15°C	Kg/m^3	---	860-900	896.1

Optical microscopy was carried out at different temperatures to detect the formed crystals in the fuel. Figure 15 illustrates the optical microscopy images for prepared biodiesel using hot-stage microscopy (HSM) at different temperatures. It can be observed that there were no detectable crystals during cooling the sample from 50°C to -6°C. Formation of several tiny needle-like crystals was observed below -9°C. The nucleation of these tiny needle-like crystals increased at -15°C whilst the size of crystals increased during further by cooling to -21°C.

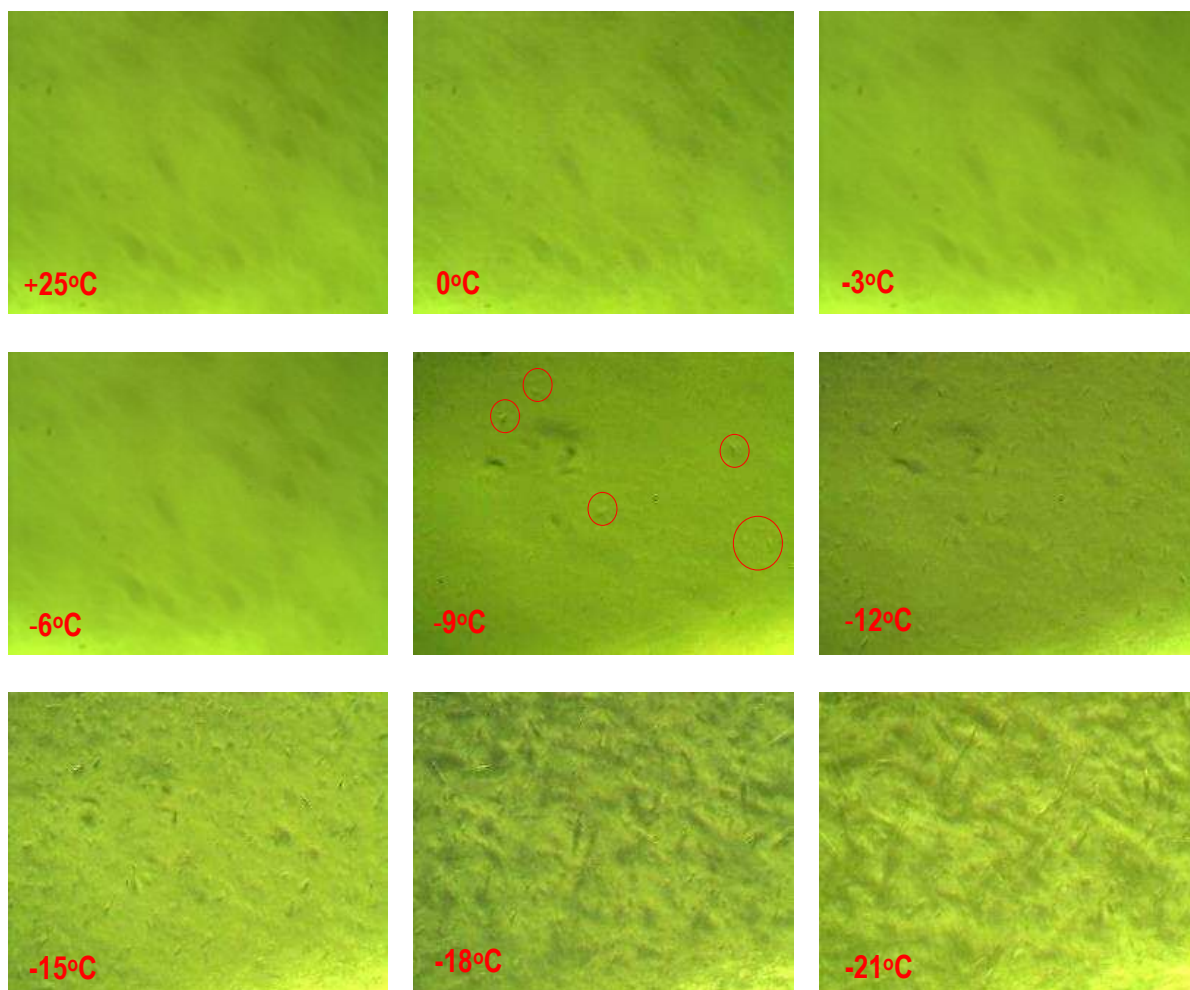


Figure 15: HSM images of the prepared biodiesel at different temperatures

3.4 Discussions

The use of chlorosulfonic acid as a reagent for sulfonation of nano-sized titanium dioxide is a promising direction for loading of sulphur species into titanium dioxide. The obtained titanium sulphate oxide or titanium oxysulfate nano-catalyst has a unique and different chemical structure

than titanium dioxide (see figure 1) and those from published work on sulphated metal oxides [30, 34, 41, 83, 95, 96]. This obvious change in the chemical structure makes the prepared $\text{Ti}(\text{SO}_4)\text{O}$ nano-catalyst more stable compared to all reported sulphated metal oxide [41] as in previous catalysis the sulphate species located on the surface of metal oxides which makes the molecule unstable [30, 34]. The stability of synthesised $\text{Ti}(\text{SO}_4)\text{O}$ nano-catalyst is due to the formation of polydentate sulphate species inside the structure of TiO_2 which also leads to a higher tolerance to high percentage of FFAs in raw material for biodiesel production. This might be due to the synergic activation of polydentate sulphate species inside the structure of TiO_2 nano-particle resulting in an increase of the Lewis and Brønsted acid sites of the nano-catalyst. The effect of different TiO_2 phases (anatase, rutile and brookite) and different SO_x loadings on the nano-sized TiO_2 template on the catalytic performance would be the subject of future studies in order to have a better understanding about the influence of Lewis and Brønsted acid sites on the yield of FAME produced from simultaneous esterification and transesterification of UCO. Furthermore, there was no evidence that the presence of absorbed carbon dioxide from atmosphere had an influence on the catalytic activity of $\text{Ti}(\text{SO}_4)\text{O}$ catalyst, but further investigations should be performed in the future studies in order to better understand the surface chemistry of this catalyst under different conditions. The amount of yield and optimised process conditions (e.g. catalyst loading, methanol to UCO molar ratio, reaction time, temperature, tolerance to FFA and catalyst reusability) have been significantly improved using the catalyst synthesised in this work as compared to the reported sulphated metal oxides [30, 34]. Finally, the conditions for simultaneous esterification and transesterification processes using previous solid acid catalysts compared to the current study are presented in Table 6.

Table 6 A comparison of reported optimum process condition for the biodiesel production using solid acid nano-catalyst

	Current study	Wang et al. [48]	Chen et al. [34]	
Oil/fat feedstock	UCO	UCO	Cottonseed oil	
Methanol to oil ratio	9:1	10:1	12:1	
Type of catalyst	Ti(SO ₄)O	SO ₄ ²⁻ /TiO ₂ /La ⁺³	SO ₄ ²⁻ /TiO ₂	SO ₄ ²⁻ /ZrO ₂
Amount of catalyst%	1.5	5	2	
Time, hr	3	1	8	
Particle size, nm	25	Not reported	Not reported	
Surface area, m ² /g	44.47	229	99.2	91.5
T, °C	75	110	230	
FAME yield %	97.1	>90	90	80
Catalyst recycled	8	5	>4	

4. CONCLUSIONS

A novel method has been used to impregnate sulphate group into TiO₂-NPs to synthesise titanium sulphate oxide or titanium oxide sulfate [Ti(SO₄)O] nano-catalyst, which can be used as a solid super acidic heterogeneous catalyst for different applications due to its high activity and stability. Different analytical techniques have been employed to differentiate the prepared Ti(SO₄)O nano-catalyst from TiO₂-NPs, all confirming a 100% Ti(SO₄)O phase. The synthesised nano catalyst and its performance has not been reported in the literature. It was found that Ti(SO₄)O can be used as a novel solid acid nano-catalyst for biodiesel production from low quality and cheap feedstock such as UCO. The effect of operating process conditions such as reaction time, catalyst loading, methanol to UCO ratio, reaction temperature, %FFA, and re-usability/stability on the biodiesel yield were examined. It was found that under certain process parameters a FAME yield of 97.1% can be achieved using Ti(SO₄)O as a nano-catalyst. The heterogeneous nano-catalyst was found to be most effective for the feedstock containing FFA up to ≤6wt%. This result indicated that the novel solid acid nano-catalyst can be used for simultaneous esterification and transesterification of UCO to biodiesel potentially reducing energy consumption in biodiesel production compared to other solid

acid catalysts. The nano-catalyst can be re-cycled and re-used up to eight times without deactivation of the active sites, overall with superior functionality, significantly improved process conditions and higher tolerance to FFA as compared to other reported metal oxide catalyst. Additionally, the produced biodiesel was analysed according to the ASTM and EN standards and the specifications are within acceptable biodiesel limits.

ACKNOWLEDGEMENTS

The authors would like to acknowledge the Kurdistan Regional Government (KRG) for providing fund (HCDP/R2-DE-23) for this research and Dr Mohammed Rehan, Dr Adrian Cunliffe, Dr Tim Comyn, Dr Michael Ward, Mrs Susanne Patel and Mr Stuart Micklethwaite for their technical assistance.

APPENDIX A. SUPPLEMENTARY DATA

Supplementary data associated with this article can be found in the online version.

REFERENCES

1. Keskin, A., M. Gürü, and D. Altıparmak, Biodiesel production from tall oil with synthesized Mn and Ni based additives: Effects of the additives on fuel consumption and emissions. *Fuel*, **2007**. 86(7-8): p. 1139-1143.
2. Ma, F. and M.A. Hanna, Biodiesel production: a review¹. *Bioresource Technology*, **1999**. 70(1): p. 1-15.
3. Salvi, B. and N. Panwar, Biodiesel resources and production technologies—A review. *Renewable and sustainable energy reviews*, **2012**. 16(6): p. 3680-3689.
4. Al- Zuhair, S., Production of biodiesel: possibilities and challenges. *Biofuels, Bioproducts and Biorefining*, **2007**. 1(1): p. 57-66.
5. Gardy, J., A. Hassanpour, X. Lai, A. Cunliffe, and M. Rehan, The influence of blending process on the quality of rapeseed oil-used cooking oil biodiesels. *Environmental Science*, **2014**. 3: p. 233-238.
6. Zhang, Y., M.A. Dubé, D.D. McLean, and M. Kates, Biodiesel production from waste cooking oil: 2. Economic assessment and sensitivity analysis. *Bioresource Technology*, **2003**. 90(3): p. 229-240.
7. Javidialesaadi, A. and S. Raeissi, Biodiesel production from high free fatty acid-content oils: Experimental investigation of the pretreatment step. *APCBEE Procedia*, **2013**. 5: p. 474-478.
8. Chai, M., Q. Tu, M. Lu, and Y.J. Yang, Esterification pretreatment of free fatty acid in biodiesel production, from laboratory to industry. *Fuel Processing Technology*, **2014**. 125: p. 106-113.
9. Lotero, E., Y. Liu, D.E. Lopez, K. Suwannakarn, D.A. Bruce, and J.G. Goodwin, Synthesis of biodiesel via acid catalysis. *Industrial & engineering chemistry research*, **2005**. 44(14): p. 5353-5363.

10. Canakci, M. and J. Van Gerpen, Biodiesel production from oils and fats with high free fatty acids. *Transactions of the ASAE*, **2001**. 44(6): p. 1429.
11. Dias, A.P.S., J. Puna, M.J.N. Correia, I. Nogueira, J. Gomes, and J. Bordado, Effect of the oil acidity on the methanolysis performances of lime catalyst biodiesel from waste frying oils (WFO). *Fuel Processing Technology*, **2013**. 116: p. 94-100.
12. Jitputti, J., B. Kitiyanan, P. Rangsunvigit, K. Bunyakiat, L. Attanatho, and P. Jenvanitpanjakul, Transesterification of crude palm kernel oil and crude coconut oil by different solid catalysts. *Chemical Engineering Journal*, **2006**. 116(1): p. 61-66.
13. Canakci, M. and J. Van Gerpen, Biodiesel production via acid catalysis. *Transactions of the ASAE-American Society of Agricultural Engineers*, **1999**. 42(5): p. 1203-1210.
14. Huber, G.W., S. Iborra, and A. Corma, Synthesis of transportation fuels from biomass: chemistry, catalysts, and engineering. *Chemical reviews*, **2006**. 106(9): p. 4044-4098.
15. Kulkarni, M.G. and A.K. Dalai, Waste cooking oil an economical source for biodiesel: a review. *Industrial & engineering chemistry research*, **2006**. 45(9): p. 2901-2913.
16. Xie, W. and T. Wang, Biodiesel production from soybean oil transesterification using tin oxide-supported WO₃ catalysts. *Fuel Processing Technology*, **2013**. 109: p. 150-155.
17. Furuta, S., H. Matsushashi, and K. Arata, Biodiesel fuel production with solid superacid catalysis in fixed bed reactor under atmospheric pressure. *Catalysis communications*, **2004**. 5(12): p. 721-723.
18. Sani, Y.M., A.O. Raji-Yahya, P.A. Alaba, A.R.A. Aziz, and W.M.A.W. Daud, Palm frond and spikelet as environmentally benign alternative solid acid catalysts for biodiesel production. *BioResources*, **2015**. 10(2): p. 3393-3408.
19. Guo, F. and Z. Fang, Biodiesel production with solid catalysts. *Biodiesel, Feedstocks and Processing Technologies*, **2011**.
20. Sharma, Y.C., B. Singh, and J. Korstad, Advancements in solid acid catalysts for ecofriendly and economically viable synthesis of biodiesel. *Biofuels, Bioproducts and Biorefining*, **2011**. 5(1): p. 69-92.
21. McNeff, C.V., L.C. McNeff, B. Yan, D.T. Nowlan, M. Rasmussen, A.E. Gyberg, B.J. Krohn, R.L. Fedie, and T.R. Hoyer, A continuous catalytic system for biodiesel production. *Applied Catalysis A: General*, **2008**. 343(1): p. 39-48.
22. Park, J.-Y., J.-S. Lee, Z.-M. Wang, and D.-K. Kim, Production and characterization of biodiesel from trap grease. *Korean Journal of Chemical Engineering*, **2010**. 27(6): p. 1791-1795.
23. Bianchi, C., D. Boffito, C. Pirola, and V. Ragaini, Low temperature de-acidification process of animal fat as a pre-step to biodiesel production. *Catalysis letters*, **2010**. 134(1-2): p. 179-183.
24. Noda, L.K., R.M. de Almeida, L.F.D. Probst, and N.S. Gonçalves, Characterization of sulfated TiO₂ prepared by the sol-gel method and its catalytic activity in the n-hexane isomerization reaction. *Journal of Molecular Catalysis A: Chemical*, **2005**. 225(1): p. 39-46.
25. Ebitani, K., J. Konishi, and H. Hattori, Skeletal isomerization of hydrocarbons over zirconium oxide promoted by platinum and sulfate ion. *Journal of Catalysis*, **1991**. 130(1): p. 257-267.
26. Jin, T., T. Yamaguchi, and K. Tanabe, Mechanism of acidity generation on sulfur-promoted metal oxides. *The Journal of Physical Chemistry*, **1986**. 90(20): p. 4794-4796.
27. Luo, X., F. Deng, L. Min, S. Luo, B. Guo, G. Zeng, and C. Au, Facile one-step synthesis of inorganic-framework molecularly imprinted TiO₂/WO₃ nanocomposite and its molecular cognitive photocatalytic degradation of target contaminant. *Environmental science & technology*, **2013**. 47(13): p. 7404-7412.
28. Sun, Y., S. Ma, Y. Du, L. Yuan, S. Wang, J. Yang, F. Deng, and F.-S. Xiao, Solvent-free preparation of nanosized sulfated zirconia with Brønsted acidic sites from a simple calcination. *The Journal of Physical Chemistry B*, **2005**. 109(7): p. 2567-2572.
29. Nayebzadeh, H., N. Saghatoleslami, A. Maskooki, and B. Vahid, Preparation of supported nanosized sulfated zirconia by strontia and assessment of its activities in the esterification of oleic acid. *Chemical and Biochemical Engineering Quarterly*, **2014**. 28(3): p. 259-265.
30. Zhao, H., P. Jiang, Y. Dong, M. Huang, and B. Liu, A high-surface-area mesoporous sulfated nano-titania solid superacid catalyst with exposed (101) facets for esterification: facile preparation and catalytic performance. *New Journal of Chemistry*, **2014**. 38(9): p. 4541-4548.
31. Rehan, M., X. Lai, and G.M. Kale, Hydrothermal synthesis of titanium dioxide nanoparticles studied employing in situ energy dispersive X-ray diffraction. *CrystEngComm*, **2011**. 13(11): p. 3725-3732.

32. Rehan, M., G.M. Kale, and X. Lai, An in situ EDXRD kinetic and mechanistic study of the hydrothermal crystallization of TiO₂ nanoparticles from nitric acid peptized sol-gel. *CrystEngComm*, **2015**. 17(9): p. 2013-2020.
33. Deng, F., Y. Liu, X. Luo, S. Wu, S. Luo, C. Au, and R. Qi, Sol-hydrothermal synthesis of inorganic-framework molecularly imprinted TiO₂/SiO₂ nanocomposite and its preferential photocatalytic degradation towards target contaminant. *Journal of hazardous materials*, **2014**. 278: p. 108-115.
34. Chen, H., B. Peng, D. Wang, and J. Wang, Biodiesel production by the transesterification of cottonseed oil by solid acid catalysts. *Frontiers of Chemical Engineering in China*, **2007**. 1(1): p. 11-15.
35. Roper-Vega, J.L., A. Aldana-Pérez, R. Gómez, and M.E. Niño-Gómez, Sulfated titania: A very active solid acid catalyst for the esterification of free fatty acids with ethanol. *Applied Catalysis A: General*, **2010**. 379(1-2): p. 24-29.
36. Shi, W. and J. Li, A deactivation mechanism of sulfated titania in the esterification of acetic acid and n-butanol. *Reaction Kinetics, Mechanisms and Catalysis*, **2014**. 111(1): p. 215-233.
37. Hosseini-Sarvari, M. and E. Sodagar, Esterification of free fatty acids (Biodiesel) using nano sulfated-titania as catalyst in solvent-free conditions. *Comptes Rendus Chimie*, **2013**. 16(3): p. 229-238.
38. Peng, B.-X., Q. Shu, J.-F. Wang, G.-R. Wang, D.-Z. Wang, and M.-H. Han, Biodiesel production from waste oil feedstocks by solid acid catalysis. *Process Safety and Environmental Protection*, **2008**. 86(6): p. 441-447.
39. Nurul Hajar, E., M. Gaanty Pragas, M. Hasbi, and A. Rahim, Biodiesel preparation from decanter cake with solid acid catalyst. *International Journal of Chemical and Environmental Engineering*, **2014**. 5(5): p. 294-296.
40. Yang, H., R. Lu, and L. Wang, Study of preparation and properties on solid superacid sulfated titania-silica nanomaterials. *Materials Letters*, **2003**. 57(5): p. 1190-1196.
41. Shao, G.N., R. Sheikh, A. Hilonga, J.E. Lee, Y.-H. Park, and H.T. Kim, Biodiesel production by sulfated mesoporous titania-silica catalysts synthesized by the sol-gel process from less expensive precursors. *Chemical Engineering Journal*, **2013**. 215-216(0): p. 600-607.
42. Garcia, C.M., S. Teixeira, L.L. Marciniuk, and U. Schuchardt, Transesterification of soybean oil catalyzed by sulfated zirconia. *Bioresource Technology*, **2008**. 99(14): p. 6608-6613.
43. Muthu, H., V. SathyaSelvabala, T. Varathachary, D. Kirupha Selvaraj, J. Nandagopal, and S. Subramanian, Synthesis of biodiesel from Neem oil using sulfated zirconia via tranesterification. *Brazilian Journal of Chemical Engineering*, **2010**. 27(4): p. 601-608.
44. Kiss, A.A., A.C. Dimian, and G. Rothenberg, Solid acid catalysts for biodiesel production-towards sustainable energy. *Advanced Synthesis & Catalysis*, **2006**. 348(1- 2): p. 75-81.
45. Boffito, D., V. Crocellà, C. Pirola, B. Neppolian, G. Cerrato, M. Ashokkumar, and C. Bianchi, Ultrasonic enhancement of the acidity, surface area and free fatty acids esterification catalytic activity of sulphated ZrO₂-TiO₂ systems. *Journal of catalysis*, **2013**. 297: p. 17-26.
46. Chavan, S.P., P. Zubaidha, S.W. Dantale, A. Keshavaraja, A. Ramaswamy, and T. Ravindranathan, Use of solid superacid (sulphated SnO₂) as efficient catalyst in facile transesterification of ketoesters. *Tetrahedron letters*, **1996**. 37(2): p. 233-236.
47. Nishikiori, H., M. Hayashibe, and T. Fujii, Visible light-photocatalytic activity of sulfate-doped titanium dioxide prepared by the Sol- Gel method. *Catalysts*, **2013**. 3(2): p. 363-377.
48. Wang, K., J. Jiang, Z. Si, and X. Liang, Biodiesel production from waste cooking oil catalyzed by solid acid SO₄²⁻/TiO₂/La³⁺. *Journal of Renewable and Sustainable Energy*, **2013**. 5(5): p. 052001.
49. Chen, F., G. Coudurier, J. Joly, and J. Védrine, Superacid and catalytic properties of sulfated zirconia. *Journal of Catalysis*, **1993**. 143(2): p. 616-626.
50. Morterra, C., G. Cerrato, C. Emanuel, and V. Bolis, On the surface acidity of some sulfate-doped ZrO₂ catalysts. *Journal of Catalysis*, **1993**. 142(2): p. 349-367.
51. Yadav, G.D. and J.J. Nair, Sulfated zirconia and its modified versions as promising catalysts for industrial processes. *Microporous and mesoporous materials*, **1999**. 33(1): p. 1-48.
52. Noda, L.K., R.M. de Almeida, N.S. Gonçalves, L.F.D. Probst, and O. Sala, TiO₂ with a high sulfate content-thermogravimetric analysis, determination of acid sites by infrared spectroscopy and catalytic activity. *Catalysis today*, **2003**. 85(1): p. 69-74.
53. LI, G., Surface modification and characterizations of TiO₂ nanoparticle. *Surface Review and Letters*, **2009**. 16(01): p. 149-151.

54. Refaat, A., Biodiesel production using solid metal oxide catalysts. *International Journal of Environmental Science & Technology*, **2011**. 8(1): p. 203-221.
55. Cui, H., K. Dwight, S. Soled, and A. Wold, Surface acidity and photocatalytic activity of Nb₂O₅/TiO₂ photocatalysts. *Journal of Solid State Chemistry*, **1995**. 115(1): p. 187-191.
56. Cheung, T.-K. and B.C. Gates, Activation of ethane in the presence of solid acids: Sulfated zirconia, iron- and manganese-promoted sulfated zirconia, and zeolites. *Journal of Catalysis*, **1997**. 168(2): p. 522-531.
57. Li, L., S. Liu, J. Xu, S. Yu, F. Liu, C. Xie, X. Ge, and J. Ren, Esterification of itaconic acid using Ln~SO₄²⁻/TiO₂-SiO₂ (Ln= La³⁺, Ce⁴⁺, Sm³⁺) as catalysts. *Journal of Molecular Catalysis A: Chemical*, **2013**. 368: p. 24-30.
58. Zhan, S., J. Jian-chun, W. Kui, and X. Jun-ming, Biodiesel production from palmitic acid esterification with rare earth composite solid acid as catalysts. *Biomass Chemical Engineering*, **2014**. 48(6): p. 25-29.
59. Sharma, R.V., C. Baroi, and A.K. Dalai, Production of biodiesel from unrefined canola oil using mesoporous sulfated Ti-SBA-15 catalyst. *Catalysis Today*, **2014**. 237: p. 3-12.
60. EN-14103, Fat and oil derivatives. Fatty acid methyl esters (FAME). Determination of ester and linolenic acid methyl ester contents. **2011**: p. 18.
61. ASTM-E203, Standard test method for water using volumetric Karl Fischer titration. ASTM international, **2008**: p. 1-10.
62. ASTM-D974, Standard test method for acid and base number by colour-indicator titration. **2012**: p. 1-7.
63. BS-EN14104, Influence of fatty acid composition of raw materials on biodiesel properties. **2003**: p. 1-12.
64. Cremlyn, R.J.W., Chlorosulfonic Acid. **2002**, Great Britain: Royal Society of Chemistry.
65. Chironna, R.J., Wet scrubbing of acidic gases <http://www.s-k.com/pdf/WetScrubbing.pdf>, **2011**: p. 1-4.
66. Stokes, A. and A. Wilson, The diffraction of X-rays by distorted crystal aggregates-I. *Proceedings of the Physical Society*, **1944**. 56(3): p. 174.
67. Bushroa, A., R. Rahbari, H. Masjuki, and M. Muhamad, Approximation of crystallite size and microstrain via XRD line broadening analysis in TiSiN thin films. *Vacuum*, **2012**. 86(8): p. 1107-1112.
68. Holzwarth, U. and N. Gibson, The Scherrer equation versus the 'Debye-Scherrer equation'. *Nat Nano*, **2011**. 6(9): p. 534-534.
69. Beranek, R. and H. Kisch, Tuning the optical and photoelectrochemical properties of surface-modified TiO₂. *Photochemical & Photobiological Sciences*, **2008**. 7(1): p. 40-48.
70. Mali, S.S., C.A. Betty, P.N. Bhosale, and P. Patil, Synthesis, characterization of hydrothermally grown MWCNT-TiO₂ photoelectrodes and their visible light absorption properties. *ECS Journal of Solid State Science and Technology*, **2012**. 1(2): p. M15-M23.
71. Sohn, J.R., S.H. Lee, P.W. Cheon, and H.W. Kim, Acidic properties and catalytic activity of titanium sulfate supported on TiO₂. *Bulletin-Korean Chemical Society*, **2004**. 25(5): p. 657-664.
72. Babou, F., G. Coudurier, and J.C. Védrine, Acidic properties of sulfated zirconia: an infrared spectroscopic study. *Journal of Catalysis*, **1995**. 152(2): p. 341-349.
73. Esteban Benito, H., T. Del Ángel Sánchez, R. García Alamilla, J. Hernández Enríquez, G. Sandoval Robles, and F. Paraguay Delgado, Synthesis and physicochemical characterization of titanium oxide and sulfated titanium oxide obtained by thermal hydrolysis of titanium tetrachloride. *Brazilian Journal of Chemical Engineering*, **2014**. 31(3): p. 737-745.
74. Thangavelu, K., R. Annamalai, and D. Arulnandhi, Preparation and characterization of nanosized TiO₂ powder by sol-gel precipitation route. *International Journal of Emerging Technology and Advanced Engineering*, **2013**. 3(1): p. 636-639.
75. Muthirulan, P., C.N. Devi, and M.M. Sundaram, TiO₂ wrapped graphene as a high performance photocatalyst for acid orange 7 dye degradation under solar/UV light irradiations. *Ceramics International*, **2014**. 40(4): p. 5945-5957.
76. Adeeva, V., J. Dehaan, J. Janchen, G. Lei, V. Schunemann, L. Vandeven, W. Sachtler, and R. Vansanten, Acid sites in sulfated and metal-promoted zirconium dioxide catalysts. *Journal of Catalysis*, **1995**. 151(2): p. 364-372.
77. Kruse, N. and S. Chenakin, XPS characterization of Au/TiO₂ catalysts: Binding energy assessment and irradiation effects. *Applied Catalysis A: General*, **2011**. 391(1): p. 367-376.

78. Barroso-Bujans, F., J.L.G. Fierro, S. Rojas, S. Sánchez-Cortes, M. Arroyo, and M.A. López-Manchado, Degree of functionalization of carbon nanofibers with benzenesulfonic groups in an acid medium. *Carbon*, **2007**. 45(8): p. 1669-1678.
79. Jensen, H., A. Soloviev, Z. Li, and E.G. Sjøgaard, XPS and FTIR investigation of the surface properties of different prepared titania nano-powders. *Applied Surface Science*, **2005**. 246(1): p. 239-249.
80. Berger, F., E. Beche, R. Berjoan, D. Klein, and A. Chambaudet, An XPS and FTIR study of SO₂ adsorption on SnO₂ surfaces. *Applied Surface Science*, **1996**. 93(1): p. 9-16.
81. Brundle, C. and A. Carley, XPS and UPS studies of the adsorption of small molecules on polycrystalline Ni films. *Faraday Discuss. Chem. Soc.*, **1975**. 60: p. 51-70.
82. Klobes, P., K. Meyer, and R.G. Munro. **2006**: US Department of Commerce, Technology Administration, National Institute of Standards and Technology.
83. Lam, M.K., K.T. Lee, and A.R. Mohamed, Sulfated tin oxide as solid superacid catalyst for transesterification of waste cooking oil: an optimization study. *Applied Catalysis B: Environmental*, **2009**. 93(1): p. 134-139.
84. Alhassan, F.H., R. Yunus, U. Rashid, K. Sirat, A. Islam, H. Lee, and Y.H. Taufiq-Yap, Production of biodiesel from mixed waste vegetable oils using ferric hydrogen sulphate as an effective reusable heterogeneous solid acid catalyst. *Applied Catalysis A: General*, **2013**. 456: p. 182-187.
85. Yang, Z. and W. Xie, Soybean oil transesterification over zinc oxide modified with alkali earth metals. *Fuel processing technology*, **2007**. 88(6): p. 631-638.
86. Boocock, D.G., S.K. Konar, V. Mao, C. Lee, and S. Buligan, Fast formation of high-purity methyl esters from vegetable oils. *Journal of the American Oil Chemists' Society*, **1998**. 75(12): p. 1167-1172.
87. Liu, X., X. Piao, Y. Wang, S. Zhu, and H. He, Calcium methoxide as a solid base catalyst for the transesterification of soybean oil to biodiesel with methanol. *Fuel*, **2008**. 87(7): p. 1076-1082.
88. Kulkarni, M.G., R. Gopinath, L.C. Meher, and A.K. Dalai, Solid acid catalyzed biodiesel production by simultaneous esterification and transesterification. *Green Chemistry*, **2006**. 8(12): p. 1056-1062.
89. Shu, Q., J. Gao, Z. Nawaz, Y. Liao, D. Wang, and J. Wang, Synthesis of biodiesel from waste vegetable oil with large amounts of free fatty acids using a carbon-based solid acid catalyst. *Applied Energy*, **2010**. 87(8): p. 2589-2596.
90. Rattanaphra, D., A. Harvey, and P. Srinophakun, Simultaneous conversion of triglyceride/free fatty acid mixtures into biodiesel using sulfated zirconia. *Topics in Catalysis*, **2010**. 53(11-12): p. 773-782.
91. Li, Y., X.-D. Zhang, L. Sun, M. Xu, W.-G. Zhou, and X.-H. Liang, Solid superacid catalyzed fatty acid methyl esters production from acid oil. *Applied Energy*, **2010**. 87(7): p. 2369-2373.
92. Shu, Q., Q. Zhang, G. Xu, Z. Nawaz, D. Wang, and J. Wang, Synthesis of biodiesel from cottonseed oil and methanol using a carbon-based solid acid catalyst. *Fuel Processing Technology*, **2009**. 90(7): p. 1002-1008.
93. Yadav, G.D. and A.D. Murkute, Preparation of a novel catalyst UDCaT-5: enhancement in activity of acid-treated zirconia—effect of treatment with chlorosulfonic acid vis-à-vis sulfuric acid. *Journal of Catalysis*, **2004**. 224(1): p. 218-223.
94. Grecea, M.L., A.C. Dimian, S. Tanase, V. Subbiah, and G. Rothenberg, Sulfated zirconia as a robust superacid catalyst for multiproduct fatty acid esterification. *Catalysis Science & Technology*, **2012**. 2(7): p. 1500-1506.
95. Roperro-Vega, J., A. Aldana-Pérez, R. Gómez, and M. Niño-Gómez, Sulfated titania [TiO₂/SO₄²⁻]: A very active solid acid catalyst for the esterification of free fatty acids with ethanol. *Applied Catalysis A: General*, **2010**. 379(1): p. 24-29.
96. Jenie, S.A., D.S. Kusuma, A. Kristiani, J.A. Laksmono, and S. Tursiloadi, Preparation and characterization of sulfated titania catalysts for the isomerisation of citronellal. *International Journal of Basic & Applied Sciences*, **2010**. 10(6): p. 5-10.